Manuscript

1 ***Full Title: Temporal relationship between systemic endothelial dysfunction and alterations in***
2 ***erythrocyte function in a murine model of chronic heart failure***
3 ***Short title: Endothelial dysfunction and erythropathy in heart failure***
4

5 Tasnim Mohaissen[1,2], Bartosz Proniewski[1], Marta Targosz- Korecka[3], Anna Bar[1], Agnieszka Kij[1],
6 Katarzyna Bulat[1], Aleksandra Wajda[1,4], Aneta Blat [1,4], Karolina Matyjaszczyk-Gwarda[1,2], Marek
7 Grosicki[1], Anna Tworzydlo[1], Magdalena Sternak[1], Kamila Wojnar-Lason[1,6], Raquel Rodrigues-Diez[5], ,
8 Agata Kubisiak[3], Ana Briones[5], Katarzyna M. Marzec[1], Stefan Chlopicki [1,6]*
9
10 *1. Jagiellonian University, Jagiellonian Center for Experimental Therapeutics (JCET),*
11 *14 Bobrzynskiego St., 30-348 Krakow, Poland*
12 *2. Jagiellonian University Medical College, Faculty of Pharmacy,*
13 *9 Medyczna St., 30-688, Krakow, Poland*
14 *3. Jagiellonian University Medical College, Faculty of Physics, Institute of Astronomy*
15 *and Applied Computer Science,*
16 *11 Lojasiewicza St., 30-348 Krakow, Poland;*
17 *4. Jagiellonian University, Faculty of Chemistry,*
18 *2 Gronostajowa St., 30-387 Krakow, Poland*
19 *5. Universidad Autónoma de Madrid, Hospital La Paz Institute for Health Research IdiPAZ*
20 *Department of Pharmacology, Faculty of Medicine, Madrid; Ciber CV Spain;*
21 *6. Jagiellonian University Medical College, Faculty of Medicine, Chair of Pharmacology,*
22 *16 Grzegorzecka St., 31-531 Krakow, Poland*
23
24 Corresponding author:
25 Prof. Stefan Chlopicki, M.D., Ph.D.
26 e-mail: stefan.chlopicki@jcet.eu
27 phone: +48 12 6645464, fax: +48 12 2974615
28 ORCID NUMBER:
29 1. Tasnim Mohaissen – 0000-0001-7495-3945
30 2. Bartosz Proniewski – 0000-0002-5138-1451
31 3. Marta Targosz- Korecka –0000-0001-5650-7255
32 4. Anna Bar- 0000-0003-0182-6501
33 5. Agnieszka Kij– 0000-0003-2233-0564
34 6. Katarzyna Bulat – 0000-0002-9326-1482
35 7. Aleksandra Wajda– 0000-0002-3433-9227
36 8. Aneta Blat – 0000-0001-8413-381X
37 9. Karolina Matyjaszczyk-Gwarda– 0000-0003-2538-6766
38 10. Marek Grosicki – 0000-0002-0122-719X
39 11. Anna Tworzydlo– 0000-0002-0638-9008
40 12. Magdalena Sternak– 0000-0001-9690-5231
41 13. Raquel Rodrigues-Diez–0000-0002-6348-1505
42 14. Kamila Wojnar-Lason– 0000-0002-9884-2032
43 15. Agata Kubisiak–0000-0003-1241-4035
44 16. Ana Briones– 0000-0001-8218-5579
45 17. Katarzyna M. Marzec – 0000-0002-8098-4622
46 18. Stefan Chlopicki – 0000-0002-2878-3858

47
48

© The Author(s) 2021. Published by Oxford University Press on behalf of the European Society of Cardiology.
This is an Open Access article distributed under the terms of the Creative Commons Attribution License
(http://creativecommons.org/licenses/by-nc/4.0/), which permits unrestricted reuse, distribution, and reproduction in any medium,
provided the original work is properly cited.

Downloaded from https://academic.oup.com/cardiovascres/advance-article/doi/10.1093/cvr/cvab306/6383136 by Uniwersytet Jagiellonsky w Krakowie user on 10 November 2021

49 **Abstract**

50 **Aims**

51 Endothelial dysfunction (ED) and red blood cell distribution width (RDW) are both prognostic
52 factors in heart failure (HF), but the relationship between them is not clear. In this study, we used a
53 unique mouse model of chronic HF driven by cardiomyocyte-specific overexpression of activated Gαq
54 protein (Tgαq*44 mice) to characterise the relationship between the development of peripheral ED and
55 the occurrence of structural nanomechanical and biochemical changes in red blood cells (RBCs).

56 **Methods and Results**

57 Systemic ED was detected *in vivo* in 8-month-old Tgαq*44 mice, as evidenced by impaired
58 acetylcholine-induced vasodilation in the aorta and increased endothelial permeability in the
59 brachiocephalic artery. ED in the aorta was associated with impaired nitric oxide (NO) production in the
60 aorta and diminished systemic NO bioavailability. ED in the aorta was also characterised by increased
61 superoxide and eicosanoid production. In 4- to 6-month-old Tgαq*44 mice, RBC size and membrane
62 composition displayed alterations that did not result in significant changes in their nanomechanical and
63 functional properties. However, 8-month-old Tgαq*44 mice presented greatly accentuated structural and
64 size changes and increased RBC stiffness. In 12-month-old Tgαq*44 mice, the erythropathy was
65 featured by severely altered RBC shape and elasticity, increased RDW, impaired RBC deformability,
66 and increased oxidative stress (GSH/GSSH ratio). Moreover, RBCs taken from 12-month-old Tgαq*44
67 mice, but not from 12-month-old FVB mice, co-incubated with aortic rings from FVB mice, induced
68 impaired endothelium-dependent vasodilation and this effect was partially reversed by an arginase
69 inhibitor (ABH, 2(S)-amino-6-boronohexanoic acid).
70

71 **Conclusion**

72 In the Tgαq*44 murine model of HF, systemic endothelial dysfunction accelerates erythropathy
73 and, conversely, erythropathy may contribute to endothelial dysfunction. These results suggest that
74 erythropathy may be regarded as a marker and a mediator of systemic endothelial dysfunction in HF. In
75 particular, targeting RBC arginase may represent a novel treatment strategy for systemic endothelial
76 dysfunction in HF. RBC arginase and possibly other RBC-mediated mechanisms may represent novel
77 therapeutic targets for systemic endothelial dysfunction in HF.
78

79 **Translational perspective**
80

81 Endothelial dysfunction (ED) and red blood cell distribution width (RDW) both have prognostic
82 value for heart failure (HF), but it is not known whether these pathologies are related. We
83 comprehensively characterized endothelial and RBC functional status in a unique murine model of
84 chronic heart failure with a prolonged time course of HF progression. Our results suggest that ED
85 accelerates erythropathy and, conversely, erythropathy may contribute to ED. Accordingly,
86 erythropathy in HF reflects ED and involves various changes (in functional, structural, nanomechanical,
87 and biochemical levels) that could have diagnostic and therapeutic significance for HF.
88
89

90 **Keywords:**
91 **Heart Failure, Endothelial dysfunction, Red Blood Cells, Erythropathy**
92
93
94
95

Downloaded from https://academic.oup.com/cardiovascres/advance-article/doi/10.1093/cvr/cvab306/6383136 by Uniwersytet Jagiellonsky w Krakowie user on 10 November 2021

96 ## 1. Introduction

97 Heart failure (HF) is an outcome of various primary and secondary incidents; in the advanced stage,
98 it results not only in impaired cardiac function but also in the development of endothelial dysfunction
99 (ED) in the peripheral circulation [1] as well as alterations in RBC function [2]. However, the relationship
100 between ED and the functional, structural, nanomechanical, and biochemical properties of RBCs in HF
101 is not clear.

102 In various diseases, including HF, ED is characterised by impaired production of NO and increased
103 production of $O_2^{\bullet -}$ [1] as well as other changes in the endothelial phenotype [1, 3]. Consistent with the
104 oxidative stress-related mechanisms of ED, antioxidant treatment strategies, including vitamin C and
105 NADPH oxidase 2 (NOX-2) and xanthine oxidase (XO) inhibitors, have been shown to improve
106 endothelial function in HF [4-6]. Various mechanisms of peripheral ED have been proposed, including a
107 decrease in shear stress linked to cardiac failure, which leads to the downregulation of endothelial nitric
108 oxide synthase (eNOS) expression and the reduction of NO production alongside increased oxidative
109 stress [3, 7]. Several contributors to ED in HF have been proposed: neurohormonal activation, with major
110 roles of angiotensin II (Ang II) [3, 8] and mineralocorticoid receptor (MR)-dependent mechanisms [7];
111 hyperactivation of the sympathetic system [1, 9]; and proinflammatory cytokines, including tumour
112 necrosis factor alpha (TNFα) and interleukin (IL)-6 [1]. Notably, the most effective pharmacological
113 treatments for HF patients, such as renin–angiotensin system (RAS) inhibitors, which include
114 angiotensin-converting enzyme (ACE) inhibitors [10], Ang II type 1 (AT1) receptor antagonists [8], and MR
115 antagonists, [11] improved endothelial function in the peripheral circulation of HF patients. Improvement
116 in peripheral ED by RAS-based treatment strategies and other treatment strategies has therapeutic
117 benefits for HF [10], including increased exercise tolerance in HF patients [12].

118 ED in peripheral circulation may have prognostic value independent of whether the HF is ischemic
119 or non-ischemic [13]. However, although abundant literature exists related to peripheral ED in HF of
120 ischemic origin [3, 14], little is known about the mechanism of ED in non-ischemic HF. Indeed, some [3, 15]
121 but not all [3, 16] authors have confirmed the development of ED in HF of non-ischemic origin.

122 Interestingly, although RBCs display physiological size heterogeneity, increased red cell
123 distribution width (RDW) is an independent predictor of the short- and long-term prognosis of HF [17, 18],
124 implicating the role of altered function of RBCs in the pathophysiology of HF. Several reciprocal
125 mechanisms between the endothelium and RBCs maintain the haemostatic balance and safeguard the
126 cardiovascular system, whereas alterations of this balance may lead to vascular pathologies such as ED
127 [19]. For example, functional alterations in RBCs induced by hyperglycaemia, diabetes [19], a high-fat diet
128 [20], malaria, and hemoglobinopathies (e.g., sickle cell diseases) contribute to the pathomechanisms of ED
129 [19], and various mechanisms have been proposed for these RBC functional changes [21, 22].

130 However, despite the knowledge that ED and RDW are both prognostic factors in HF, the
131 relationship between alterations in RBC function and the development of peripheral ED in HF is not
132 clear. Although patients with HF present alterations in several hemorheological properties as well as
133 impairment of peripheral blood flow [23], it is not known whether these pathologies are related, whether
134 they occur simultaneously, or whether one precedes the other. To the best of our knowledge, the link
135 between RBC alterations and endothelial function in HF has not been defined previously.

136 To fill this gap, we characterised the development of peripheral ED and the progression of
137 functional, structural, nanomechanical, and biochemical alterations of RBCs, taking advantage of a
138 unique murine model of chronic HF (Tgαq*44 mice) generated by cardiomyocyte-specific
139 overactivation of the Gαq protein, which imitates excessive neurohormonal cardiac activation [24]. This
140 model is relevant to the pathophysiology of human HF and is characterised by prolonged HF
141 progression, with distinct early and late stages of the disease that have been described previously [25, 26].

Downloaded from https://academic.oup.com/cardiovascres/advance-article/doi/10.1093/cvr/cvab306/6383136 by Uniwersytet Jagiellonsky w Krakowie user on 10 November 2021

142 Thus, this model seemed well suited to characterise the temporal associations between alterations in
143 endothelial and RBC function, two phenomena involved in HF pathophysiology.
144

145 2. Methods

146 2.1. Animals

147 Female Tgαq*44 mice, a model of heart failure (HF) initially developed by Mende et al. [24, 27],
148 and FVB (wild-type) mice were bred in the Animal Laboratory of the Medical Research Centre of
149 the Polish Academy of Sciences (Warsaw, Poland). Transgenic = αq*44 mice based on the FVB
150 strain express an HA epitope-tagged, constitutively active mutated αq (HAα*q) under the control of
151 the α-MHC promoter and represent a unique model of chronic HF [24, 27]. All animal procedures were
152 in accordance with the Guide for the Care and Use of Laboratory Animals published by the US
153 National Institutes of Health (NIH Publication No. 85–23, revised 1985) as well as with the local
154 Ethical Committee on Animal Experiments in Krakow. Mice were fed a standard chow diet and kept
155 in 12:12 light–dark conditions.

156 2.1 Assessment of endothelium-dependent vasodilation and endothelial permeability
157 *in vivo* by magnetic resonance imaging

158 Endothelial function and permeability *in vivo* were assessed as described previously [28-30].
159 Briefly, endothelium-dependent vasodilation *in vivo* was assessed by measuring the response to
160 acetylcholine (Ach, Sigma-Aldrich, Poznań Poland: 50 µl, 16.6 mg/kg, i.p.) in the abdominal aorta
161 (AA) and by flow-mediated dilatation (FMD) in response to reactive hyperaemia (after 5 min vessel
162 occlusion) in the femoral artery (FA) [29]. Changes in endothelial function were expressed as changes
163 in the vessel volume [30]. Moreover, changes in endothelial permeability were assessed by relaxation
164 time (T_1) map measurements in the brachiocephalic artery (BCA) using the variable flip angle
165 technique [31, 32] before and 30 minutes after intravenous administration of a unique formulation of
166 gadolinium contained in the liposome (gadodiamide in the liposome, concentration of formulation:
167 (287 mg/mL, 4.5 mL/kg, intravenous (i.v.)).

168 2.2 Aorta isolation

169 Mice were euthanized intraperitoneally with a mixture of ketamine and xylazine in doses of 100
170 and 10 mg/kg body weight (b.w.), respectively. Subsequently, the aorta was removed and placed in
171 cold Krebs–Henseleit solution (KB) bubbled with a 95% O_2/5% CO_2 mixture (pH = 7.4). Aortic
172 segments used for NO, superoxide, or eicosanoid production were immediately placed in fresh KB
173 or frozen at −80 °C.

174 2.2.1 Assessment of endothelium-dependent and -independent vasodilation
175 *ex vivo* in wire myograph system

176 Aortic rings were mounted in a Mulvany myograph system (620 M, Danish Myo Technology,
177 Denmark), followed by assessment of the endothelium-dependent and independent vasodilation *ex*
178 *vivo*, carried out as previously described [33]. To study RBC-induced endothelial dysfunction, RBCs
179 taken from 12-month-old Tgαq*44 or 12-month-old FVB mice were isolated [34], diluted with serum-
180 free culture medium to a hematocrit of 5%, and were incubated with aortic rings isolated from 12-
181 month-old Tgαq*44 or 12-month-old FVB mice in cell culture incubator at 37 °C with 5% carbon
182 dioxide for 18 h in the absence or presence of 100 uM of 2(S)-amino-6-boronohexanoic acid (ABH).

183 2.2.2 Assessment of eicosanoid production in isolated aortic rings by LC-MS/MS

184 Aortic rings were added to a 24-well plate containing KB. The plate was placed into a BIO-V
185 gas treatment chamber (Noxygen Science, Elzach, Germany), where it remained for 15 min under
186 CO_2 flow at 37 °C. After pre-incubation, the aortic rings were placed into 500 mL of fresh KB, and
187 100 mL samples of the incubation buffer were taken after 3 min and 45 min of incubation. The

Downloaded from https://academic.oup.com/cardiovascres/advance-article/doi/10.1093/cvr/cvab306/6383136 by Uniwersytet Jagiellonsky w Krakowie user on 10 November 2021

188 concentrations of 6-keto prostaglandin F1α (6-keto $PGF_{1α}$), as well as prostaglandin E_2 and D_2 (PGE_2
189 and PGD_2) and 15-hydroxyeicosatetraenoic acid (15-HETE) in the aorta effluents, were examined
190 by a liquid chromatograph UFLC Nexera (Shimadzu, Kyoto, Japan) coupled to a triple quadrupole
191 mass spectrometer QTRAP 5500 (SCIEX, Framingham, MA, USA) following the methodology
192 previously described [35]. The biosynthesis of PGI_2 and TXA_2 were assessed based on the
193 concentration of their stable metabolites 6-keto PGF_{1a} and TXB_2, respectively. Results are presented
194 as the difference between the concentration assessed after 3 min and 45 min incubation.

195 **2.2.3 Assessment of NO and $O_2^{\bullet-}$ production in the isolated aorta by electron paramagnetic**
196 **resonance spectroscopy**

197 Nitric oxide production in the isolated aorta was measured by electron paramagnetic resonance
198 (EPR) with the cell-permeable NO spin trapping agent diethyldithiocarbamate (DETC), as described
199 previously [36].

200 **2.2.4 Assessment of TNFα and IL-1β gene expression by qRT-PCR**

201 Total RNA was extracted from the aorta of Tgaq*44 and FVB mice with TRI Reagent (Sigma-
202 Aldrich, St. Louis, MO, USA) following the manufacturer's procedures, as described previously [37].

203 **2.3 Blood and RBC analysis**

204 Depending on the applied method of analysis the blood samples, isolated RBCs or RBC
205 membranes were studied. Whole blood samples were collected from the right ventricle using
206 a syringe containing additional anticoagulant (heparin). The details of RBC isolation from the whole
207 blood and RBC membrane isolation (prepared by overnight freezing of RBCs suspended in 0.9%
208 NaCl, haematocrit = 10%) are presented in the Supplemental Materials (SM).

209 **2.3.1 Blood count, blood biochemistry, and determination of NO metabolites**

210 A whole blood sample was used for blood count analysis using an automatic haematology
211 analyser ABC Vet (Horiba, Kyoto, Japan). Plasma obtained after centrifugation (acceleration: 1000
212 ×*g*, run time: 10 min, 4 °C) was used for measuring the lipid profile with an ABX Pentra biochemical
213 analyser (Horiba Medical Kyoto, Japan).

214 Measurement of nitrate (NO_3^-) and nitrite (NO_2^-) concentrations in the plasma was performed
215 using an ENO-20 NOx analyser (Eicom Corp., Kyoto, Japan), applying a liquid chromatography
216 method with post-column derivatisation using Griess reagent [38]. The packed RBCs remaining after
217 centrifugation were used for GSH and GSSG concentration measurement as well as nitrosyl
218 haemoglobin (HbNO) detection with EPR spectroscopy [39].

219 **2.3.2 Assessment of RBC shape and nanomechanics by AFM**

220 Erythrocyte shape and elasticity were measured using a NanoWizard 3 (JPK Instruments,
221 Berlin, Germany) AFM microscope. All measurements were performed using a pyramidal AFM
222 probe attached to V-shaped silicon nitride cantilevers with a spring constant of 0.01 N/m (MLCT-
223 C, Veeco Probes, Camarillo, CA, USA). The force mapping mode was used for both topography
224 and elasticity measurements. The elastic moduli of RBCs were calculated using the Hertz–Sneddon
225 model with the approximation for a paraboloidal probe. Data were analysed using JPKSPM Data
226 Processing software. The aspect ratio was defined as the ratio between two perpendicular main axes
227 of the RBCs (i.e., the length and width of the cell) [40].

228 **2.3.3 Assessment of RBC deformability by Rheoscan**

229 Erythrocyte deformability was measured using a microfluidic RheoScan AnD 300
230 (RheoMeditech, Seoul, South Korea) following the protocol suggested by the manufacturer. RBC
231 deformation was quantified at a shear stress of 20 Pa in terms of the maximum elongation index
232 (EI_{max}) [40].

Downloaded from https://academic.oup.com/cardiovascres/advance-article/doi/10.1093/cvr/cvab306/6383136 by Uniwersytet Jagiellonsky w Krakowie user on 10 November 2021

233 #### 2.3.4 Assessment of RBC by flow cytometry

234 RBCs and reticulocytes were analysed with a BD LSR II flow cytometer (BD Biosciences, 235 Oxford, UK) and stained against anti-mouse TER-119 PerCP/Cy5.5 (BioLegend, San Diego, United 236 States) and anti-mouse CD71 APC (BioLegend, San Diego, United States) antibodies and annexin V 237 FITC (antibody dilution 1:100, stained for 30 min at room temperature). For each sample 100 000 000 238 events were acquired in log mode for forward side scatter (FSC), side scatter (SSC) and fluorescent 239 signals. Data were analysed using BD FACSDiva Software (BD Biosciences, Oxford, UK). RBC and 240 reticulocytes were gated according to their characteristic log FCS, log SSC, and fluorescent signals.

241 #### 2.3.5 Assessment of GSH and GSSG concentration in RBCs by capillary electrophoresis

242 GSH and GSSG concentrations were measured using a P/ACE MDQ capillary electrophoresis 243 (CE) system (Beckman Coulter, Fullerton, CA, USA) with 32 Karat software (ver. 8.0, Beckman 244 Coulter, Fullerton, CA, USA) as previously described [41].

245 #### 2.3.6 Assessment of biochemical content of RBC membranes by Raman spectroscopy and 246 Fourier transform infrared spectroscopy–attenuated total reflectance

247 Isolated RBC membranes were deposited on CaF2 slides, air-dried for 30 min, and examined 248 with Raman spectroscopy (RS) followed by Fourier transform infrared spectroscopy–attenuated 249 total reflectance (FTIR–ATR). The exact methodology of these measurements and data analysis 250 were reported and validated in our previous studies[40, 42].

251 **Details of methods are given in SM.**

252 ### 2.4 Statistical analysis

253 Statistical analyses were performed using GraphPad Prism 8.4 (GraphPad Software) software. 254 The results are presented as box plots (median, Q1, Q3, interquartile range, and outliers). Tgαq*44 255 mice in different phases of HF were compared with age-matched control groups and analysed using 256 two-way ANOVA. The normality of the distribution and homogeneity of variance were tested using 257 the Shapiro–Wilk and F-tests, respectively. When these assumptions were violated, nonparametric 258 tests were performed (Kruskal–Wallis ANOVA). Probability values (P) of less than 0.05 were 259 considered statistically significant.

260

261 ## 3. Results

262 ### 3.1 Development of systemic endothelial dysfunction in Tgαq*44 mice, *in vivo* MRI-based 263 measurements

264 MRI-based assessment of endothelium-dependent response *in vivo* revealed that in 8-month-old 265 Tgαq*44 mice, acetylcholine (Ach)-induced vasodilation in the abdominal aorta (AA) was impaired, 266 whereas in older mice (10- to 12-month-old Tgαq*44 mice), Ach-induced vasodilation was completely 267 lost and changed to vasoconstriction (Fig. 1A, $p < 0.05$). ED in 8-month-old Tgαq*44 mice was 268 confirmed by increased endothelial permeability measured *in vivo* by MRI with the use of the Npx50 269 parameter of endothelial permeability as described previously [43]. The T_1 signal near the BCA lumen 270 after intravenous injection of gadolinium-containing liposomes was increased in Tgαq*44 mice aged 8 271 months and older compared with age-matched FVB mice (Fig. 1B). By contrast, flow-mediated 272 vasodilation (FMD) in the FA was fully preserved in 8-month-old Tgαq*44 mice compared with that in 273 age-matched FVB mice. FMD in the FA was also slightly impaired in 12-month-old Tgαq*44 mice, but 274 this difference did not reach statistical significance (Fig. 1C).

275 ### 3.2 Development of ED in the aorta of Tgαq*44 mice; *ex vivo* measurements

276 In 10- and 12-month-old Tgαq*44 mice, but not 6- and 8-month-old Tgαq*44 mice, Ach-induced 277 endothelium-dependent vasodilation was decreased compared with the age-matched FVB mice (Fig. 278 1D–1G), whereas endothelium-independent vasodilation induced by sodium nitroprusside (SNP) was 279 fully preserved in all experimental groups of Tgαq*44 mice and age-matched FVB mice (Fig. 1H–1K).

Downloaded from https://academic.oup.com/cardiovascres/advance-article/doi/10.1093/cvr/cvab306/6383136 by Uniwersytet Jagiellonsky w Krakowie user on 10 November 2021

280 ### 3.3 Systemic bioavailability of NO in Tgαq*44 mice

281 Systemic ED in Tgαq*44 mice was not associated with a reduction in the NO_2^- concentration in
282 plasma. However, the NO_3^- plasma concentration decreased in 10- to 12-month-old Tgαq*44 mice
283 compared with that of FVB mice (Table 1). In contrast to the lack of decreased plasma NO_2^-
284 concentration, the HbNO content in RBCs substantially decreased in 12-month-old Tgαq*44 mice
285 compared with that in the RBCs of age-matched FVB mice (Table 1). Tgαq*44 mice did not display
286 any changes in blood biochemistry compared with age-matched FVB mice until the age of 12 months,
287 when the plasma concentration of the urea significantly increased, whereas the total cholesterol (TC)
288 and HDL cholesterol plasma levels modesty decreased in Tgαq*44 mice compared with the levels in
289 FVB mice (Table 1).

290 ### 3.4 Alterations in NO/$O_2^{\bullet-}$ balance and in eicosanoid production in the aorta of Tgαq*44 mice

291 ED in the aorta of 12-month-old Tgαq*44 mice was accompanied by a decrease in stimulated NO
292 production in *ex vivo* aortas measured by EPR (Fig. 2A) compared with the age-matched FVB mice.
293 Furthermore, impairment of endothelial functional response in the aorta was associated with increased
294 $O_2^{\bullet-}$ production in 12-month-old Tgαq*44 mice compared with that in age-matched FVB (Fig. 2B).

295 In 12-month-old Tgαq*44 mice, but not in younger Tgαq*44 mice, the production of 6-keto
296 $PGF_{1\alpha}$, PGE_2, PGD_2, and 15-HETE in the aorta was higher than in age-matched FVB mice (Fig. 2C–F).
297 However, TNFα (Fig. 2G) and IL-1β (Fig. 2H) mRNA gene expression in the aorta did not differ
298 between the 12-month-old Tgαq*44 mice and age-matched FVB mice.

299 ### 3.5 Basic characterisation of alterations in RBs in Tgαq*44 mice

300 Alterations in RBC indices were not associated with significant differences in haemoglobin (HGB),
301 haematocrit (HCT), or white blood cell (WBC) and platelet (PLT) counts between Tgαq*44 mice and
302 age-matched FVB mice (Table 1). Mean corpuscular haemoglobin (MCH) and mean corpuscular
303 haemoglobin concentration (MCHC) were lower in 8- to 12-month-old Tgαq*44 mice than in age-
304 matched FVB mice, but not in the early stage of HF (Table 1), whereas mean corpuscular volume (MCV)
305 was significantly lower in 4- to 12-month-old Tgαq*44 mice than in age-matched FVB mice (Figure
306 3A). RDW was significantly increased in 10- to 12-month-old Tgαq*44 mice (Fig. 3B) compared with
307 that in age-matched FVB mice. There was no statistically significant difference in the extent of
308 reticulocytosis between Tgαq*44 and FVB mice (Fig. 3C). The annexin V staining did not differ
309 between Tgαq*44 and FVB mice at the age of 4 months and was slightly decreased in 12-month-old
310 Tgαq*44 mice compared with that in age-matched FVB mice (Fig. 3D).

311 Total glutathione, GSH, and GSSG in RBCs did not show statistically significant differences
312 between Tgαq*44 mice and FVB mice (data not shown), but the GSH/GSSG ratio was significantly
313 lower in 12-month-old Tgαq*44 mice compared with that in age-matched FVB mice (Fig. 3E). RBC
314 deformability measured at a high shear stress (20 Pa) displayed a marked decrease in 12-month-old
315 Tgαq*44 mice compared with that in age-matched FVB mice (Fig. 3F).

316 ### 3.6 Characterisation of alterations in topography and nanomechanics of RBCs in Tgαq*44 mice
317 ### by AFM

318 The examples of RBC images in Fig. 4 reflect high variability of RBC shape during HF progression,
319 from a normal biconcave shape to discocytes and spherocytes with irregular symmetry. In the control
320 sample from 4-month-old FVB mice, a characteristic biconcave or doughnut shape of RBCs was
321 observed. In 12-month-old FVB mice (Fig. 4B), the deformation of the blood cells was manifested by a
322 slight loss of symmetry in the height of the blood cells. In Tgαq*44 mice, more pronounced changes in
323 RBC shape were observed (Fig. 4C–H). In the youngest mice, a change in the shape of the RBCs was
324 manifested either by an increase in the central part of the blood cell or a large change in the RBC height
325 profile symmetry. In 8-month-old Tgαq*44 mice, significant cell deformation resulting in aspect ratio

Downloaded from https://academic.oup.com/cardiovascres/advance-article/doi/10.1093/cvr/cvab306/6383136 by Uniwersytet Jagiellonsky w Krakowie user on 10 November 2021

326 modification and diminished biconcave shape were noted. These changes were even more pronounced
327 in 12-month-old Tgαq*44 mice.
328 The quantitative results of the aspect ratio are presented in Fig. 5A, and the measured cell elastic
329 moduli are presented in Fig. 5B. In 8-, 10-, and 12-month-old Tgαq*44 mice, both parameters were
330 significantly increased compared with the parameters in age-matched control mice. In 4- and 6-month-
331 old Tgαq*44 mice, the differences did not reach statistical significance. Interestingly, there was a
332 significant negative correlation between endothelial function (measured *in vivo* by MRI) and RBC
333 elasticity (measured by AFM) in Tgαq*44 mice, and this correlation was not observed in FVB mice
334 (Fig. 5C). As shown in Fig. 5D, the increased RBC aspect ratio was correlated with increased stiffness
335 in both Tgaq*44 and FVB mice along with ageing; however, Tgaq*44 mice displayed a marked shift
336 towards a higher aspect ratio and a higher elastic moduli value.

337 **3.7 Effects of RBCs isolated from Tgαq*44 mice during early and end-stage HF on endothelium-**
338 **dependent vasodilation, *ex vivo* measurements**

339 As shown in Fig. 5E, RBCs isolated from 12-month-old Tgαq*44 mice that were coincubated with
340 aortic rings induced the impairment of endothelium-dependent vasodilation, whereas endothelial-
341 independent vasodilation was preserved. By contrast, RBCs isolated from 12-month-old FVB mice did
342 not impair the endothelial function in the aortic rings (Fig. 5E). Interestingly, in the presence of ABH
343 (100 μM), an inhibitor of arginase, detrimental effect of RBCs taken from 12-month-old Tgαq*44 mice
344 on endothelial function in the aorta was prevented. The effect of ABH was significant only for the
345 highest concentration of Ach (10 μM), but there were no effects of ABH on SNP-induced relaxation
346 (Fig. 5F and 5H).

347 **3.8 Characterisation of alterations in biochemical contents of RBC membranes in Tgαq*44**
348 **mice by vibrational spectroscopy**

349 In the RBC membranes of Tgαq*44 mice compared with age-matched FVB mice, FTIR-based
350 analysis revealed that stretching vibrations of the =CH groups (band at 3013 cm^{-1}) and antisymmetric
351 stretching vibrations of the PO_2^- groups (band at 1235 cm^{-1}) differed significantly, indicating a reduction
352 in phospholipid content (Fig. 6A) and a decrease in the unsaturation of membrane lipids (Fig. 6D). These
353 changes were statistically significant in 4-month-old Tgαq*44 mice compared with FVB mice, and a
354 similar degree of difference was observed in 12-month-old Tgαq*44 mice compared with FVB mice.
355 RS did not reveal changes in total lipid proteins (Fig. 6C) or the fraction of esters, including cholesterol
356 esters (Fig. 6B and F), in RBC membranes obtained from 4- and 12-month-old Tgαq*44 compared with
357 age-matched FVB mice, whereas the overall protein content did not undergo changes (Fig. 6E) as
358 determined by FTIR and RS-based assessment.
359
360 **4. Discussion**
361
362 In the present work, we used a comprehensive methodology to assess the endothelial and RBC
363 functional status and characterise the temporal relationships between the development of ED and the
364 development of erythropathy in Tgαq*44 mice, a unique murine model of chronic HF with a prolonged
365 time course of the HF progression. In contrast to most animal models, in which the transition from
366 compensated to uncompensated chronic heart failure (CHF) is relatively rapid, the Tgαq*44 murine
367 model is characterised by a delayed progression to end-stage heart failure [24-26, 44]. The prolonged window
368 of HF progression in Tgαq*44 mice from adaptive to end-stage HF allowed us to discover that RBC
369 alterations occurred very early in HF pathophysiology and progressed substantially with HF
370 progression. In particular, HF-linked erythropathy in Tgαq*44 mice accelerated substantially and was
371 correlated with the progression of systemic ED. Increased RBC stiffness assessed by AFM was
372 correlated with impaired endothelial function assessed *in vivo* by MRI. Finally, RBCs in late-stage
373 erythropathy induced ED when co-incubated with aorta samples from FVB mice, whereas RBCs in early

Downloaded from https://academic.oup.com/cardiovascres/advance-article/doi/10.1093/cvr/cvab306/6383136 by Uniwersytet Jagiellonsky w Krakowie user on 10 November 2021

374 erythropathy stages did not. These results suggest a possible reciprocal relationship between RBC
375 alterations and endothelial function in HF: systemic ED accelerates erythropathy and, conversely,
376 erythropathy may contribute to ED. Such a reciprocal relationship was previously postulated to occur
377 in other diseases [19] but was not previously characterized in HF.

378 The major advantage of our experimental approach was that it assessed endothelial function by
379 the application of an MRI-based method *in vivo,* a method that was validated in our previous studies [28,
380 29, 43]. This approach appeared to be more sensitive for detecting the early phase of ED (in 8-month-old
381 Tgαq*44 mice) compared with classical isolated vessel studies *ex vivo* (in 10-month-old Tgαq*44 mice)
382 and the direct measurement of NO/$O_2^{\bullet-}$ balance (in 12-month-old Tgαq*44 mice). Using our
383 comprehensive methodological approach, we demonstrated that systemic ED was present in 8-month-
384 old Tgαq*44 mice (impaired Ach-induced vasodilation and increased endothelial permeability *in vivo*)
385 and progressed further in 10-month-old Tgαq*44 mice, as evidenced by impaired Ach-induced
386 vasodilation with preserved SNP response in the aorta *ex vivo*. Furthermore, in 12-month-old Tgαq*44
387 mice, impaired NO production and increased $O_2^{\bullet-}$ production, phenomena that have been reported
388 previously in HF [3-5], were observed through biochemical measurements of the aorta.

389 Interestingly, in contrast to the impaired endothelial function in the aorta, the FMD response in the
390 FA *in vivo* seemed to be largely preserved until end-stage HF. Previous studies have demonstrated
391 heterogeneity in the response of the aorta and the FA in ageing and diabetes [45, 46] As age increased,
392 relaxation in response to Ach was reduced in the aorta, whereas in the FA response was fully preserved
393 [47]. In addition, in db/db mice, the vasodilatory response to Ach was impaired in the FA but not in the
394 aorta [48]. Finally, in a model of HF induced by myocardial infarction [45, 46] FMD in the FA was heavily
395 impaired, while the response to Ach was only moderately affected. Comparing the results of these
396 studies with our findings underscores the heterogeneous response of the endothelium to HF progression
397 in the conduit vessels in ischemic and non-ischemic HF and reveals a difference in response depending
398 on the vascular bed and stimulus used [46, 49].

399 Interestingly, impaired Ach-induced NO-dependent vasodilation in the aorta was associated with a
400 progressive reduction in plasma concentration of nitrate (8- to 12-month-old Tgαq*44 mice), whereas
401 the concentration of nitrite remained unchanged, which suggests the activation of the nitrate–nitrite–NO
402 reductive pathway, an alternative compensatory source that maintains NO bioavailability [2]. However,
403 as the HbNO content in RBCs substantially decreased in 12-month-old Tgαq*44 mice in late-stage HF
404 in this model, the systemic NO bioavailability eventually fell substantially despite the activation of the
405 nitrite reductive pathway.

406 Concomitantly, in 12-month-old Tgαq*44 mice, ED was characterised by increased generation of
407 cyclooxygenase-derived eicosanoids, such as PGD_2 and PGI_2 (assessed as its metabolite 6-keto $PGF_{1\alpha}$),
408 which may play a compensatory role [50]. In turn, increased vascular PGE_2 could contribute to vascular
409 inflammation and ED [37].

410 The comprehensive nature of RBC analysis based on the numerous methods, including AFM and
411 vibrational spectroscopy, adapted in the present work allowed us to obtain unprecedented insight into
412 structural, functional, nanomechanical, and biochemical changes in RBCs related to the progression of
413 ED in HF. We demonstrated that RBCs displayed mild alterations as early as 4 months old in Tgαq*44
414 mice. These changes included a reduction in MCV, suggesting early RBC anisocytosis in HF; a slightly
415 altered aspect ratio (assessed by AFM topography), indicating an early RBC shape alteration; and a
416 decrease in phospholipid content and unsaturated lipids in RBC membranes (assessed by vibrational
417 spectroscopy), implying early RBC membranes changes. Still, these changed did not result in
418 statistically significant alterations in the nanomechanics or deformability of RBCs at this stage of HF.
419 However, even at this HF stage, some RBCs displayed notable changes in elasticity. Notably, several
420 parameters of erythropathy were significantly accentuated in 8-month-old Tgαq*44 mice, including

Downloaded from https://academic.oup.com/cardiovascres/advance-article/doi/10.1093/cvr/cvab306/6383136 by Uniwersytet Jagiellonsky w Krakowie user on 10 November 2021

421 structural changes (increased AFM-based aspect ratio indicative of the presence of ellipsoidal RBCs)
422 and nanomechanical alterations (increased RBC elasticity modulus). In 12-month-old Tgαq*44 mice,
423 HF-linked erythropathy was characterised not only by severely altered RBC shape and elasticity but
424 also by increased RDW, impaired RBC deformability, and oxidative stress (GSH/GSSH ratio).

425 Taken together, in Tgαq*44 mice, HF-linked erythropathy was characterised by early changes
426 in RBC size and membrane composition but preserved RBC function, which could suggest early changes
427 in erythropoiesis, most likely of a compensatory nature [51]. HF-linked erythropathy involved altered
428 shape and elasticity (AFM topography and nanoindentation), altered biochemical RBC homeostasis
429 (oxidant stress), and, finally, impaired deformability of RBCs tested using the clinically used Rheoscan
430 system (see Fig. 7). Of note, alterations in RBC status based on Rheoscan, GSH/GSSG, and RDW
431 parameters were detected at very late stages of erythropathy, in contrast to alterations in RBC
432 membranes and changes in their nanomechanical profile detected in the early phase of HF. Interestingly,
433 alterations in the biochemical profile of RBC membranes and the size of RBCs shown here displayed a
434 distinct pattern compared with atherosclerosis [40] or HF of ischemic origin [52]. In a previous study by our
435 group [40] using ApoE/LDLR$^{-/-}$ mice, phospholipids and unsaturated lipids decreased with the progression
436 of atherosclerosis; however, the total lipid content and MCV was higher, without significant differences
437 in RDW, in ApoE/LDLR$^{-/-}$ mice compared with age-matched controls. In the current study, levels of
438 phospholipids and lipid unsaturation in RBC membranes were significantly lower even in the early
439 phase of HF in 4- and 6-month-old Tgαq*44 mice, without changes in total lipid content. MCV values
440 were reduced and further decreased with the progression of HF, whereas a significant increase in RDW
441 values was observed in the late stage of HF in 12-month-old Tgαq*44 mice only. These results agree
442 with the accepted notion that the modification of the lipid composition in the RBC membranes results
443 in changes in their shape and elasticity. Furthermore, our results revealed that HF-related erythropathy
444 displayed different types of RBC alterations compared with atherosclerosis-related changes [40].

445 Most importantly, our results showed that HF-linked erythropathy in Tgαq*44 mice was
446 temporarily linked with the progression of ED. Moreover, the progression of erythropathy seems to be
447 correlated with progressive impairment of endothelial function (alterations in RBC elasticity were
448 correlated with progressive impairment of Ach-induced NO-dependent vasodilation in the aorta).

449 Of note, in 8-month-old Tgαq*44 mice, a severe pattern of HF-linked erythropathy was present.
450 This stage of HF in Tgαq*44 mice was characterised by the presence of ED, whereas cardiac function
451 was relatively compensated compared with late-stage HF in 12-month-old Tgαq*44 mice, which was
452 characterised by severe impairment of basal cardiac function, cardiac reserve, and exercise capacity [26].
453 Taken together, our findings support the theory that endothelial function plays a key role in maintaining
454 RBC haemostasis. As such, systemic ED may accelerate erythropathy. However, erythropathy has
455 detrimental effects on endothelial function in other diseases [19]. This study also provided evidence
456 supporting such a possibility. In advanced erythropathy, RBCs taken from 12-month-old Tgαq*44 mice
457 and co-incubated with isolated aorta rings induced impairment in endothelium-dependent relaxation in
458 the *ex vivo* assay, and this effect was prevented by the inhibition of arginase. Of note, a similar
459 experimental approach was previously used to show the contribution of diabetic erythropathy to the
460 development of ED in diabetes [53]. Interestingly, Pernow et al. discovered that the activation of arginase
461 I in RBCs contributed to the development of ED in diabetes [19]. Arginase in RBCs was also suggested to
462 mediate endothelial dysfunction associated with pre-eclampsia[54].

463 Interestingly, in our study, ABH (an inhibitor of arginase types I and II) prevented RBC-induced
464 impairment of endothelial function. This effect was however only detectable for the highest
465 concentration of Ach. Pernow et. al [55] show that murine RBC expresses only arginase type I, but not
466 arginase type II. Thus, our data suggest that impaired NO-dependent function in Tgaq*44 mice may be
467 partially due to arginase I activity in RBC, but of course, this is just one of a number of mechanisms

Downloaded from https://academic.oup.com/cardiovascres/advance-article/doi/10.1093/cvr/cvab306/6383136 by Uniwersytet Jagiellonsky w Krakowie user on 10 November 2021

468 that could contribute to systemic endothelial dysfunction in HF. Also, erythropathy could contribute to
469 endothelial dysfunction by mechanisms independent on arginase [21, 22, 56-58].
470 Taken together, there seems to be a reciprocal relationship between endothelial function and
471 RBC hemostasis in HF as suggested previously for diabetes [19]. Systemic ED accelerates erythropathy
472 and *vice versa*, erythropathy may contribute to ED. These results suggest that erythropathy may be
473 regarded as a marker and a mediator of systemic ED in HF. Furthermore, RBC arginase and possibly
474 other RBC-mediated mechanisms may represent novel therapeutic targets for systemic endothelial
475 dysfunction in HF.
476 Previous studies showed that RBCs express functional eNOS protein, which is closely
477 correlated with FMD in humans [56], confirming a strong association between RBC functional status and
478 endothelial function. Indeed, changes in RBC membranes could lead to increased RBC adhesion to
479 endothelial cells [19, 57]; for example, in diabetes, malaria, and hemoglobinopathies [19]. Increased RBC
480 adhesion to the endothelium may lead to impaired tissue microcirculation [21, 22]. Furthermore, amylin
481 deposited on RBCs [58] or myeloperoxidase activation on the RBC surface could also contribute to
482 oxidative stress and impairment of NO-dependent relaxation [59]. It remains to be established whether any
483 of these RBC-mediated mechanisms also contribute to ED in HF. Moreover, previous studies of HF-
484 linked erythropathy, defined as RDW, predicted a poor prognosis in patients with clinical HF [17].
485 Interestingly, it was suggested that HF-linked erythropathy was independent of systemic inflammation,
486 kidney function, and numerous other studied variables, including NT-proBNP (a good biomarker of HF
487 progression) [60], leaving the underlying mechanisms of the relationship between RDW and HF unclear
488 [17, 18]. In agreement with these findings in Tgaq*44 mice, systemic inflammation, erythropoietin, and
489 kidney failure are also unlikely mechanisms of HF-linked erythropathy because the first two were not
490 altered in 4-, 8-, and 12-month-old Tgαq*44 mice (results not shown) and the latter was a late
491 phenomenon, as evidenced by the fact that the plasma urea concentration increased only in 12-month-
492 old Tgaq*44 mice.
493 Our study has several limitations. As in previous work using this model [24, 27], only female mice
494 were used, so we cannot be sure whether the findings of this work are also relevant to male Tgαq*44
495 mice. To confirm the detrimental effects of RBCs on endothelial function *ex vivo*, the isolated aorta was
496 used similarly as in methodology described previously [19], but we cannot be sure to what extent RBCs
497 contribute to ED in HF *in vivo* since *ex vivo* studies are not able to fully mimic the *in vivo* setting. Finally,
498 although we provided experimental evidence that RBCs in advanced erythropathy induce impaired
499 endothelial function, and we postulated arginase in RBC to be partially involved, further experiments
500 with more selective arginase inhibitors and tissue-specific arginase knock-out are mandatory to delineate
501 in detail the importance of arginase in impaired NO-dependent function in Tgaq*44 mice.
502 In conclusion, HF-linked erythropathy in Tgaq*44 mice involved progressive alterations on
503 functional, structural, nanomechanical, and biochemical levels. The temporal relationship and
504 correlation between the progression of HF-linked erythropathy and the progression of impairment of
505 vascular NO-dependent function in Tgαq*44 mice suggest that erythropathy may be a marker and a
506 mediator of vascular dysfunction in HF. To the best of our knowledge, this relationship was not
507 demonstrated previously in the context of HF, despite a wealth of evidence that RDW has prognostic
508 significance in HF. Surprisingly, HF represents a disease in which targeting RBCs may represent a novel
509 treatment modality to reverse systemic endothelial dysfunction.
510
511 **5. Funding**
512 This work was supported by the National Science Centre, Poland mainly by PRELUDIUM 15 grant
513 (no. UMO 2018/29/N/NZ24/02915) (TM) and partial by SYMFONIA 3 grant (no. DEC-
514 2015/16/W/NZ4/00070) (SCH) and an OPUS 12 grant (no. UMO 2016/23/B/ST4/00795) (KMM).
515

Downloaded from https://academic.oup.com/cardiovascres/advance-article/doi/10.1093/cvr/cvab306/6383136 by Uniwersytet Jagiellonsky w Krakowie user on 10 November 2021

516 **6. Author Contribution Statement**
517
518 TM and SCH conceived and designed the study. TM, BP, MT-K, ABar. AK, KB, AW, ABlat, KM-
519 G, MG, AT, MS, RR-D, KW-L, AKubi performed experiments. TM, BP, MT-K, ABar, AW, ABlat
520 analyzed the data. TM, MT-K prepared the figures. TM and SCH wrote the draft of the manuscript.
521 KMM, AB critically revised the manuscript for important intellectual content. KMM edited and revised
522 the manuscript. TM and SCH wrote the final version of the manuscript. All authors read and approved
523 the final version of the manuscript.
524
525 **7. A conflict of interest**
526 The authors declare no competing interests.
527
528 **8. Data Availability**
529 The data underlying this article are available on reasonable request to the corresponding author.
530
531
532 **9. References**
533
534 1. Cortese-Krott MM, Kelm M. Endothelial nitric oxide synthase in red blood cells: key
535 to a new erythrocrine function? *Redox Biol* 2014;**2**:251-258.
536 2. Gevaert AB, Lemmens K, Vrints CJ, Van Craenenbroeck EM. Targeting Endothelial
537 Function to Treat Heart Failure with Preserved Ejection Fraction: The Promise of
538 Exercise Training. *Oxid Med Cell Longev* 2017;**2017**:4865756.
539 3. Giannitsi S, Bougiakli M, Bechlioulis A, Naka K. Endothelial dysfunction and heart
540 failure: A review of the existing bibliography with emphasis on flow mediated
541 dilation. *JRSM Cardiovasc Dis* 2019;**8**:2048004019843047.
542 4. Baldus S, Köster R, Chumley P, Heitzer T, Rudolph V, Ostad MA, Warnholtz A,
543 Staude HJ, Thuneke F, Koss K, Berger J, Meinertz T, Freeman BA, Münzel T.
544 Oxypurinol improves coronary and peripheral endothelial function in patients with
545 coronary artery disease. *Free Radic Biol Med* 2005;**39**:1184-1190.
546 5. Erbs S, Gielen S, Linke A, Möbius-Winkler S, Adams V, Baither Y, Schuler G,
547 Hambrecht R. Improvement of peripheral endothelial dysfunction by acute vitamin C
548 application: different effects in patients with coronary artery disease, ischemic, and
549 dilated cardiomyopathy. *Am Heart J* 2003;**146**:280-285.
550 6. Zhang M, Perino A, Ghigo A, Hirsch E, Shah AM. NADPH oxidases in heart failure:
551 poachers or gamekeepers? *Antioxid Redox Signal* 2013;**18**:1024-1041.
552 7. Bauersachs J, Widder JD. Endothelial dysfunction in heart failure. *Pharmacol Rep*
553 2008;**60**:119-126.
554 8. Schäfer A, Fraccarollo D, Tas P, Schmidt I, Ertl G, Bauersachs J. Endothelial
555 dysfunction in congestive heart failure: ACE inhibition vs. angiotensin II antagonism.
556 *Eur J Heart Fail* 2004;**6**:151-159.
557 9. Battault S, Meziat C, Nascimento A, Braud L, Gayrard S, Legros C, De Nardi F, Drai
558 J, Cazorla O, Thireau J, Meyer G, Reboul C. Vascular endothelial function masks
559 increased sympathetic vasopressor activity in rats with metabolic syndrome. *Am J*
560 *Physiol Heart Circ Physiol* 2018;**314**:H497-H507.
561 10. Joannides R, Bizet-Nafeh C, Costentin A, Iacob M, Derumeaux G, Cribier A, Thuillez
562 C. Chronic ACE inhibition enhances the endothelial control of arterial mechanics and
563 flow-dependent vasodilatation in heart failure. *Hypertension* 2001;**38**:1446-1450.
564 11. Bauersachs J, Heck M, Fraccarollo D, Hildemann SK, Ertl G, Wehling M, Christ M.
565 Addition of spironolactone to angiotensin-converting enzyme inhibition in heart
566 failure improves endothelial vasomotor dysfunction: role of vascular superoxide anion

Downloaded from https://academic.oup.com/cardiovascres/advance-article/doi/10.1093/cvr/cvab306/6383136 by Uniwersytet Jagiellonsky w Krakowie user on 10 November 2021

567 formation and endothelial nitric oxide synthase expression. *J Am Coll Cardiol*
568 2002;**39**:351-358.
569 12. Hambrecht R, Fiehn E, Weigl C, Gielen S, Hamann C, Kaiser R, Yu J, Adams V,
570 Niebauer J, Schuler G. Regular physical exercise corrects endothelial dysfunction and
571 improves exercise capacity in patients with chronic heart failure. *Circulation*
572 1998;**98**:2709-2715.
573 13. Fischer D, Rossa S, Landmesser U, Spiekermann S, Engberding N, Hornig B, Drexler
574 H. Endothelial dysfunction in patients with chronic heart failure is independently
575 associated with increased incidence of hospitalization, cardiac transplantation, or
576 death. *Eur Heart J* 2005;**26**:65-69.
577 14. Klosinska M, Rudzinski T, Grzelak P, Stefanczyk L, Drozdz J, Krzeminska-Pakula M.
578 Endothelium-dependent and -independent vasodilation is more attenuated in ischaemic
579 than in non-ischaemic heart failure. *Eur J Heart Fail* 2009;**11**:765-770.
580 15. Patel AR, Kuvin JT, Pandian NG, Smith JJ, Udelson JE, Mendelsohn ME, Konstam
581 MA, Karas RH. Heart failure etiology affects peripheral vascular endothelial function
582 after cardiac transplantation. *J Am Coll Cardiol* 2001;**37**:195-200.
583 16. Shah A, Gkaliagkousi E, Ritter JM, Ferro A. Endothelial function and arterial
584 compliance are not impaired in subjects with heart failure of non-ischemic origin. *J*
585 *Card Fail* 2010;**16**:114-120.
586 17. Borné Y, Smith JG, Melander O, Hedblad B, Engström G. Red cell distribution width
587 and risk for first hospitalization due to heart failure: a population-based cohort study.
588 *Eur J Heart Fail* 2011;**13**:1355-1361.
589 18. Pascual-Figal DA, Bonaque JC, Redondo B, Caro C, Manzano-Fernandez S, Sánchez-
590 Mas J, Garrido IP, Valdes M. Red blood cell distribution width predicts long-term
591 outcome regardless of anaemia status in acute heart failure patients. *Eur J Heart Fail*
592 2009;**11**:840-846.
593 19. Pernow J, Mahdi A, Yang J, Zhou Z. Red blood cell dysfunction: a new player in
594 cardiovascular disease. *Cardiovasc Res* 2019;**115**:1596-1605.
595 20. Unruh D, Srinivasan R, Benson T, Haigh S, Coyle D, Batra N, Keil R, Sturm R,
596 Blanco V, Palascak M, Franco RS, Tong W, Chatterjee T, Hui DY, Davidson WS,
597 Aronow BJ, Kalfa T, Manka D, Peairs A, Blomkalns A, Fulton DJ, Brittain JE,
598 Weintraub NL, Bogdanov VY. Red Blood Cell Dysfunction Induced by High-Fat
599 Diet: Potential Implications for Obesity-Related Atherosclerosis. *Circulation*
600 2015;**132**:1898-1908.
601 21. Anniss AM, Sparrow RL. Variable adhesion of different red blood cell products to
602 activated vascular endothelium under flow conditions. *Am J Hematol* 2007;**82**:439-
603 445.
604 22. Shiu YT, McIntire LV. In vitro studies of erythrocyte-vascular endothelium
605 interactions. *Ann Biomed Eng* 2003;**31**:1299-1313.
606 23. Tikhomirova I, Petrochenko E, Muravyov A, Malysheva Y, Petrochenko A,
607 Yakusevich V, Oslyakova A. Microcirculation and blood rheology abnormalities in
608 chronic heart failure. *Clin Hemorheol Microcirc* 2017;**65**:383-391.
609 24. Mende U, Semsarian C, Martins DC, Kagen A, Duffy C, Schoen FJ, Neer EJ. Dilated
610 cardiomyopathy in two transgenic mouse lines expressing activated G protein
611 alpha(q): lack of correlation between phospholipase C activation and the phenotype. *J*
612 *Mol Cell Cardiol* 2001;**33**:1477-1491.
613 25. Mackiewicz U, Czarnowska E, Brudek M, Pająk B, Duda M, Emanuel K, Csanyi G,
614 Fedorowicz A, Grochal E, Tyrankiewicz U, Skórka T, Mende U, Lewartowski B,
615 Chłopicki S. Preserved cardiomyocyte function and altered desmin pattern in

Downloaded from https://academic.oup.com/cardiovascres/advance-article/doi/10.1093/cvr/cvab306/6383136 by Uniwersytet Jagiellonsky w Krakowie user on 10 November 2021

616 transgenic mouse model of dilated cardiomyopathy. *J Mol Cell Cardiol* 2012;**52**:978-
617 987.
618 26. Tyrankiewicz U, Olkowicz M, Skórka T, Jablonska M, Orzylowska A, Bar A, Gonet
619 M, Berkowicz P, Jasinski K, Zoladz JA, Smolenski RT, Chlopicki S. Activation
620 pattern of ACE2/Ang-(1-7) and ACE/Ang II pathway in course of heart failure
621 assessed by multiparametric MRI in vivo in Tgαq*44 mice. *J Appl Physiol (1985)*
622 2018;**124**:52-65.
623 27. Mende U, Kagen A, Cohen A, Aramburu J, Schoen FJ, Neer EJ. Transient cardiac
624 expression of constitutively active Galphaq leads to hypertrophy and dilated
625 cardiomyopathy by calcineurin-dependent and independent pathways. *Proc Natl Acad*
626 *Sci U S A* 1998;**95**:13893-13898.
627 28. Bar A, Targosz-Korecka M, Suraj J, Proniewski B, Jasztal A, Marczyk B, Sternak M,
628 Przybyło M, Kurpińska A, Walczak M, Kostogrys RB, Szymonski M, Chlopicki S.
629 Degradation of Glycocalyx and Multiple Manifestations of Endothelial Dysfunction
630 Coincide in the Early Phase of Endothelial Dysfunction Before Atherosclerotic Plaque
631 Development in Apolipoprotein E/Low-Density Lipoprotein Receptor-Deficient Mice.
632 *J Am Heart Assoc* 2019;**8**:e011171.
633 29. Sternak M, Bar A, Adamski MG, Mohaissen T, Marczyk B, Kieronska A, Stojak M,
634 Kus K, Tarjus A, Jaisser F, Chlopicki S. The Deletion of Endothelial Sodium Channel
635 α (αENaC) Impairs Endothelium-Dependent Vasodilation and Endothelial Barrier
636 Integrity in Endotoxemia. *Front Pharmacol* 2018;**9**:178.
637 30. Bar A, Skórka T, Jasiński K, Sternak M, Bartel Ż, Tyrankiewicz U, Chlopicki S.
638 Retrospectively gated MRI for in vivo assessment of endothelium-dependent
639 vasodilatation and endothelial permeability in murine models of endothelial
640 dysfunction. *NMR Biomed* 2016;**29**:1088-1097.
641 31. Cheng HL, Wright GA. Rapid high-resolution T(1) mapping by variable flip angles:
642 accurate and precise measurements in the presence of radiofrequency field
643 inhomogeneity. *Magn Reson Med* 2006;**55**:566-574.
644 32. Wang J, Qiu M, Kim H, Constable RT. T1 measurements incorporating flip angle
645 calibration and correction in vivo. *J Magn Reson* 2006;**182**:283-292.
646 33. Fedorowicz A, Buczek E, Mateuszuk Ł, Czarnowska E, Sitek B, Jasztal A, Chmura-
647 Skirlińska A, Dib M, Steven S, Daiber A, Chlopicki S. Comparison of Pulmonary and
648 Systemic NO- and PGI. *Oxid Med Cell Longev* 2018;**2018**:4036709.
649 34. Zhou Z, Mahdi A, Tratsiakovich Y, Zahorán S, Kövamees O, Nordin F, Uribe
650 Gonzalez AE, Alvarsson M, Östenson CG, Andersson DC, Hedin U, Hermesz E,
651 Lundberg JO, Yang J, Pernow J. Erythrocytes From Patients With Type 2 Diabetes
652 Induce Endothelial Dysfunction Via Arginase I. *J Am Coll Cardiol* 2018;**72**:769-780.
653 35. Kij A, Kus K, Czyzynska-Cichon I, Chlopicki S, Walczak M. Development and
654 validation of a rapid, specific and sensitive LC-MS/MS bioanalytical method for
655 eicosanoid quantification - assessment of arachidonic acid metabolic pathway activity
656 in hypertensive rats. *Biochimie* 2020;**171-172**:223-232.
657 36. Proniewski B, Kij A, Sitek B, Kelley EE, Chlopicki S. Multiorgan Development of
658 Oxidative and Nitrosative Stress in LPS-Induced Endotoxemia in C57Bl/6 Mice:
659 DHE-Based. *Oxid Med Cell Longev* 2019;**2019**:7838406.
660 37. Avendaño MS, García-Redondo AB, Zalba G, González-Amor M, Aguado A,
661 Martínez-Revelles S, Beltrán LM, Camacho M, Cachofeiro V, Alonso MJ, Salaices
662 M, Briones AM. mPGES-1 (Microsomal Prostaglandin E Synthase-1) Mediates
663 Vascular Dysfunction in Hypertension Through Oxidative Stress. *Hypertension*
664 2018;**72**:492-502.

Downloaded from https://academic.oup.com/cardiovascres/advance-article/doi/10.1093/cvr/cvab306/6383136 by Uniwersytet Jagiellonsky w Krakowie user on 10 November 2021

665 38. Przyborowski K, Proniewski B, Czarny J, Smeda M, Sitek B, Zakrzewska A, Zoladz
666 JA, Chlopicki S. Vascular Nitric Oxide-Superoxide Balance and Thrombus Formation
667 after Acute Exercise. *Med Sci Sports Exerc* 2018;**50**:1405-1412.
668 39. Frolow M, Drozdz A, Kowalewska A, Nizankowski R, Chlopicki S. Comprehensive
669 assessment of vascular health in patients; towards endothelium-guided therapy.
670 *Pharmacol Rep* 2015;**67**:786-792.
671 40. Dybas J, Bulat K, Blat A, Mohaissen T, Wajda A, Mardyla M, Kaczmarska M,
672 Franczyk-Zarow M, Malek K, Chlopicki S, Marzec KM. Age-related and
673 atherosclerosis-related erythropathy in ApoE/LDLR. *Biochim Biophys Acta Mol Basis*
674 *Dis* 2020:165972.
675 41. Hempe JM, Ory-Ascani J. Simultaneous analysis of reduced glutathione and
676 glutathione disulfide by capillary zone electrophoresis. *Electrophoresis* 2014;**35**:967-
677 971.
678 42. Blat A, Wiercigroch E, Smeda M, Wislocka A, Chlopicki S, Malek K. Fourier
679 transform infrared spectroscopic signature of blood plasma in the progression of breast
680 cancer with simultaneous metastasis to lungs. *J Biophotonics* 2019;**12**:e201900067.
681 43. Bar A, Kieronska-Rudek A, Proniewski B, Suraj-Prażmowska J, Czamara K, Marczyk
682 B, Matyjaszczyk-Gwarda K, Jasztal A, Kuś E, Majka Z, Kaczor A, Kurpińska A,
683 Walczak M, Pieterman EJ, Princen HMG, Chlopicki S. In Vivo Magnetic Resonance
684 Imaging-Based Detection of Heterogeneous Endothelial Response in Thoracic and
685 Abdominal Aorta to Short-Term High-Fat Diet Ascribed to Differences in
686 Perivascular Adipose Tissue in Mice. *J Am Heart Assoc* 2020;**9**:e016929.
687 44. Elas M, Bielanska J, Pustelny K, Plonka PM, Drelicharz L, Skorka T, Tyrankiewicz
688 U, Wozniak M, Heinze-Paluchowska S, Walski M, Wojnar L, Fortin D, Ventura-
689 Clapier R, Chlopicki S. Detection of mitochondrial dysfunction by EPR technique in
690 mouse model of dilated cardiomyopathy. *Free Radic Biol Med* 2008;**45**:321-328.
691 45. Maupoint J, Besnier M, Gomez E, Bouhzam N, Henry JP, Boyer O, Nicol L, Mulder
692 P, Martinet J, Richard V. Selective Vascular Endothelial Protection Reduces Cardiac
693 Dysfunction in Chronic Heart Failure. *Circ Heart Fail* 2016;**9**:e002895.
694 46. Vercauteren M, Remy E, Devaux C, Dautreaux B, Henry JP, Bauer F, Mulder P,
695 Hooft van Huijsduijnen R, Bombrun A, Thuillez C, Richard V. Improvement of
696 peripheral endothelial dysfunction by protein tyrosine phosphatase inhibitors in heart
697 failure. *Circulation* 2006;**114**:2498-2507.
698 47. Barton M, Cosentino F, Brandes RP, Moreau P, Shaw S, Lüscher TF. Anatomic
699 heterogeneity of vascular aging: role of nitric oxide and endothelin. *Hypertension*
700 1997;**30**:817-824.
701 48. Sallam NA, Laher I. Redox Signaling and Regional Heterogeneity of Endothelial
702 Dysfunction in. *Int J Mol Sci* 2020;**21**.
703 49. Liu Y, Bubolz AH, Mendoza S, Zhang DX, Gutterman DD. H2O2 is the transferrable
704 factor mediating flow-induced dilation in human coronary arterioles. *Circ Res*
705 2011;**108**:566-573.
706 50. Félétou M, Huang Y, Vanhoutte PM. Endothelium-mediated control of vascular tone:
707 COX-1 and COX-2 products. *Br J Pharmacol* 2011;**164**:894-912.
708 51. Semenza GL. Involvement of oxygen-sensing pathways in physiologic and pathologic
709 erythropoiesis. *Blood* 2009;**114**:2015-2019.
710 52. Tang HY, Wang CH, Ho HY, Wu PT, Hung CL, Huang CY, Wu PR, Yeh YH, Cheng
711 ML. Lipidomics reveals accumulation of the oxidized cholesterol in erythrocytes of
712 heart failure patients. *Redox Biol* 2018;**14**:499-508.

Downloaded from https://academic.oup.com/cardiovascres/advance-article/doi/10.1093/cvr/cvab306/6383136 by Uniwersytet Jagiellonsky w Krakowie user on 10 November 2021

53. Mahdi A, Jiao T, Tratsiakovich Y, Yang J, Östenson CG, Pernow J, Zhou Z. Altered Purinergic Receptor Sensitivity in Type 2 Diabetes-Associated Endothelial Dysfunction and Up_4 A-Mediated Vascular Contraction. *Int J Mol Sci* 2018;**19**.
54. McCann Haworth SM, Zhuge Z, Nihlén C, Von Rosen MF, Weitzberg E, Lundberg JO, Krmar RT, Nasiell J, Carlström M. Red blood cells from patients with pre-eclampsia induce endothelial dysfunction. *J Hypertens* 2021;**39**:1628-1641.
55. Yang J, Gonon AT, Sjöquist PO, Lundberg JO, Pernow J. Arginase regulates red blood cell nitric oxide synthase and export of cardioprotective nitric oxide bioactivity. *Proc Natl Acad Sci U S A* 2013;**110**:15049-15054.
56. Verma N, Liu M, Ly H, Loria A, Campbell KS, Bush H, Kern PA, Jose PA, Taegtmeyer H, Bers DM, Despa S, Goldstein LB, Murray AJ, Despa F. Diabetic microcirculatory disturbances and pathologic erythropoiesis are provoked by deposition of amyloid-forming amylin in red blood cells and capillaries. *Kidney Int* 2020;**97**:143-155.
57. Adam M, Gajdova S, Kolarova H, Kubala L, Lau D, Geisler A, Ravekes T, Rudolph V, Tsao PS, Blankenberg S, Baldus S, Klinke A. Red blood cells serve as intravascular carriers of myeloperoxidase. *J Mol Cell Cardiol* 2014;**74**:353-363.
58. Helms CC, Gladwin MT, Kim-Shapiro DB. Erythrocytes and Vascular Function: Oxygen and Nitric Oxide. *Front Physiol* 2018;**9**:125.
59. Cortese-Krott MM, Rodriguez-Mateos A, Sansone R, Kuhnle GG, Thasian-Sivarajah S, Krenz T, Horn P, Krisp C, Wolters D, Heiß C, Kröncke KD, Hogg N, Feelisch M, Kelm M. Human red blood cells at work: identification and visualization of erythrocytic eNOS activity in health and disease. *Blood* 2012;**120**:4229-4237.
60. Argan O, Ural D, Karauzum K, Bozyel S, Aktas M, Karauzum IY, Kozdag G, Agacdiken Agir A. Elevated levels of vitamin B12 in chronic stable heart failure: a marker for subclinical liver damage and impaired prognosis. *Ther Clin Risk Manag* 2018;**14**:1067-1073.

Downloaded from https://academic.oup.com/cardiovascres/advance-article/doi/10.1093/cvr/cvab306/6383136 by Uniwersytet Jagiellonsky w Krakowie user on 10 November 2021

762 *Figure Legends:*

763

764 ***Table 1. Body mass, blood count, lipid profile and NO metabolism in Tgαq*44 mice compared with***
765 ***age-matched FVB mice.*** *Body mass (n = 9–13), Blood biochemistry (n = 7): TC (total cholesterol),*
766 *HDL (high-density lipoprotein), LDL (low-density lipoprotein), TG (triglycerides), creatinine, and urea.*
767 *Blood count (n = 9–13): WBC (white blood cells), PLT (platelets), RBC (red blood cells), HGB*
768 *(haemoglobin), HCT (haematocrit), MCH (mean corpuscular haemoglobin), and MCHC (mean*
769 *corpuscular haemoglobin concentration). NO metabolism (n = 5–13): Nitrite (NO_2), Nitrate (NO_3^-)*
770 *concentration, and HbNO (nitrosylhaemoglobin) in 4-, 8-, 10-, and 12-month-old Tgαq*44 mice vs. age-*
771 *matched FVB controls mice. Normality was assessed using a Shapiro–Wilk test. Results are presented*
772 *as means ± SD, *p < 0.05, **p < 0.01, ***p < 0.001 ****p < 0.0001, Tgαq*44 mice and age-matched*
773 *FVB controls compared using two-way ANOVA with post hoc Sidak test or nonparametric Kruskal–*
774 *Wallis test (NO_2^- and NO_3^-).*

775

776 ***Figure 1. Peripheral vascular endothelial dysfunction (ED) with the progression of HF in Tgαq*44***
777 ***mice compared with age-matched FVB mice.*** In vivo *changes in the end- diastolic volume of the*
778 *abdominal aorta (AA) 25 minutes after acetylcholine administration (n = 4–6) (**A**). Changes in*
779 *endothelial permeability are described as Npx50 value, after injection of gadolinium-rich liposome*
780 *contrast agent (BCA-permeability (PER) (n = 5–6) (**B**).* In vivo *changes in the volume of the FA (FMD)*
781 *after 5-minute vessel occlusion (n = 5–6) (**C**).* Ex vivo: *Relaxation of the aorta rings in response to*
782 *increasing doses of acetylcholine (Ach) (**D–G**) and sodium nitroprusside (SNP) (**H–K**) (n = 6–8) in 4-,*
783 *8-, 10-, and 12-month-old Tgαq*44 mice vs. age-matched FVB controls mice. Normality was assessed*
784 *using a Shapiro–Wilk test. Results are presented as box plots (median, Q1, Q3, whiskers indicate*
785 *minimum/maximum), Q1 and Q3 indicate the 25th and 75th percentiles, respectively (A–C), mean ±*
786 *SEM (D–K). *p < 0.05, **p < 0.01, ***p < 0.001 ****p < 0.0001, Tgαq*44 mice and age-matched*
787 *FVB controls compared using two-way ANOVA with post hoc Sidak test.*

788

789 ***Figure 2. Alterations in NO/superoxide balance, eicosanoid, and tumour necrosis factor alpha***
790 ***(TNFα) and Interleukin-1β (IL-1β) gene expression with the progression of HF in Tgαq*44 mice***
791 ***compared with age-matched FVB mice.*** *NO production in the isolated aorta (n = 5–13) (A), $O_2^{\bullet -}$*
792 *production in aortic rings (n=5–13) (B), basal production of eicosanoid (n = 5–6) 6-keto $PGF_{1\alpha}$ (C),*
793 *PGE_2 (D), PGD_2 (E), and 15-HETE (F) detected in the effluent after 45 minutes of incubation of isolated*
794 *aortic rings. TNF (G) and IL- 1β (H) gene expression (n = 5–6) in the aorta in 4-, 8-, 10-, and 12-month-*
795 *old Tgαq*44 mice vs. FVB controls. Normality was assessed using a Shapiro–Wilk test. Results are*
796 *presented as box plots (median, Q1, Q3, whiskers indicate minimum/maximum). Q1 and Q3 indicate the*
797 *25th and 75th percentiles, respectively. *p < 0.05, **p < 0.01, ***p < 0.001, ****p < 0.0001, Tgαq*44*
798 *mice compared with age-matched FVB controls using two-way ANOVA with post hoc Sidak test.*

799

800 ***Figure 3. Alteration in blood count, apoptotic RBCs, GSH/GSSG ratio (oxidative stress), and***
801 ***erythrocyte deformability with the progression of HF in Tgαq*44 mice compared with age-matched***
802 ***FVB mice.*** *The mean corpuscular volume (MCV) (n = 11–12) (**A**) and red blood cell distribution width*
803 *(RDW) (n = 10–12) (**B**) in the blood in 4-, 6-, 8-, 10- and 12-month-old Tgαq*44 mice vs FVB controls*
804 *mice. The percentage of RBCs and reticulocytes (n = 9–11) (**C**), and the number of apoptotic RBCs (n*
805 *= 9–11) (**D**) in the blood samples in 4- and 12-month-old Tgαq*44 mice vs. FVB mice. The glutathione*
806 *redox ratio ($GSSG \cdot GSH^{-1}$) (n = 7–10) (**E**), RBCs deformability (n = 7–12) (**F**) at shear stress (20 Pa)*
807 *in the RBCs in 4-, 8-, 10-, and 12-month-old Tgαq*44 mice vs. FVB controls mice. Normality was*
808 *assessed using a Shapiro- Wilk test. Results are presented as box plots (median, Q1, Q3, whiskers*

Downloaded from https://academic.oup.com/cardiovascres/advance-article/doi/10.1093/cvr/cvab306/6383136 by Uniwersytet Jagiellonsky w Krakowie user on 10 November 2021

809 *indicate minimum/maximum). Q1 and Q3 indicate the 25th and 75th percentiles, respectively.* $*p < 0.05$,
810 $**p < 0.01$, $***p < 0.001$, $****p < 0.0001$, *Tgαq*44 mice compared with age-matched FVB controls*
811 *using two-way ANOVA with post hoc Sidak test.*
812
813 ***Figure 4. Variability of RBC shape along the progression of HF in Tgαq*44 mice compared with***
814 ***age-matched FVB mice.*** *Examples of RBC images taken for 4-month-old (A) and 12-month-old (B)*
815 *FVB mice (control sample). Examples of RBC shape changes observed for 4-month-old (C–D), 8-month-*
816 *old (E–F), and 12-month-old (G–H) Tgαq*44 mice. Plots below AFM images show cross-sections along*
817 *the marked lines.*
818
819 ***Figure 5. Changes in the aspect ratio and elastic moduli of RBCs with the progression of HF in***
820 ***Tgαq*44 mice compared with age-matched FVB mice (A–D). Effects of RBC co-incubation with the***
821 ***aorta on endothelium-dependent relaxation (E–H).*** *Cell aspect ratio of RBCs (n = 5–6, 6 repeats per*
822 *mouse) (**A**), elastic modulus of RBCs (n = 5–6, 6 repeats per mouse) (**B**), correlation between elasticity*
823 *modulus in RBCs and ED (**C**), correlation between aspect ratio and elasticity modulus in RBCs (**D**) in*
824 *4-, 6-, 8-, 10- and 12-month-old Tgαq*44 mice vs FVB controls mice. Endothelium-dependent relaxation*
825 *induced by acetylcholine (ACh) (**E**) and endothelium-independent relaxation induced by sodium*
826 *nitroprusside (SNP) (F) in the aortas isolated from 4-month-old FVB mice co-incubated with RBCs*
827 *isolated from 12-month-old Tgαq*44 mice (RBCs-12-m-Tgαq*44) or 12-month-FVB mice (RBCs-12-*
828 *m-FVB) (n = 5–6). Effects of (2(S)-amino-6-boronohexanoic acid (ABH) on responses of Ach (**G**) and*
829 *SNP (**H**) are shown from the same experimental setting (n = 5–6). Normality was assessed using a*
830 *Shapiro–Wilk test.Results are presented as box plots (median, Q1, Q3, whiskers indicate*
831 *minimum/maximum), Q and Q3 indicate the 25th and 75th percentiles, respectively (A–B), mean ± SEM*
832 *(E–H).* $*p < 0.05$, $**p < 0.01$, $***p < 0.001$, $****p < 0.0001$, *Tgαq*44 mice compared with age-*
833 *matched FVB controls,* $^{+}p < 0.05$, $^{++}p < 0.01$, $^{+++}p < 0.001$, *Control vs RBCs-12-m-Tgαq*44,* $^{\$\$\$}p <$
834 0.001 *RBCs-12-m-Tgαq*44 vs RBCs-12-m-FVB- ABH,* $^{\#\#}p < 0.01$ *RBCs-12-m-Tgαq*44 vs RBCs-12-m-*
835 *Tgαq*44 - ABH using two-way ANOVA with post hoc Sidak test.*
836
837 ***Figure 6. Changes of biochemical components of RBC membranes with the progression of HF in***
838 ***Tgαq*44 mice compared with age-matched FVB mice.*** *The integration regions for IR bands:*
839 *phospholipids (**A**): at 1236* cm^{-1} *(1269–1194* cm^{-1}*), cholesterol esters (**B**), proteins (**C**): amide I (1672–*
840 *1608), amide II (1562–1503* cm^{-1}*), unsaturation (**D**) 3013* cm^{-1} *(3001–2980* cm^{-1}*), lipid/protein ratio*
841 *(**E**), ester/protein ratio (**F**). N =5 – 6 mice per experiment (total n = 32–36) for 4- and 12-month-old*
842 *mice. In 8- and 10-month-old mice, one independent experiment was carried out on pooled RBCs*
843 *obtained from n = 12 mice per group (5 average spectra from randomly measured points: 30 for RS*
844 *and 5 for IR). Normality was assessed using a Shapiro–Wilk test. Results are presented as box plots*
845 *(median, Q1, Q3, whiskers indicate minimum/maximum), Q1 and Q3 indicate the 25th and 75th*
846 *percentiles, respectively (A–B), mean ± SEM (E–H).* $*p<0.05$, $**p<0.01$, $***p<0.001$, $****p<0.0001$,
847 *Tgαq*44 mice compared with age-matched FVB controls, two-way ANOVA with post hoc Sidak test.*
848
849 ***Figure 7. Schematic diagram summarizing the temporal relationship between the progression of***
850 ***endothelial dysfunction and erythropathy in Tgαq*44 mice, representing the murine model of chronic***
851 ***heart failure****. At early stages of HF (4 months) a decrease in MCV (*$p < 0.05$*), biochemical alterations*
852 *in RBC membranes (decreased phospholipids (*$p < 0.0001$*), and unsaturation (*$p < 0.001$*)) were present;*
853 *however, these changes were not associated with functional alterations of RBCs and endothelial*
854 *function was fully preserved. At the transition phase of HF, apart from a decrease in MCV (*$p < 0.0001$*),*
855 *a substantial increase in RBC stiffness (*$p < 0.0001$*), and alteration in RBC shape were noted (early*
856 *phase of erythropathy), as well as impaired endothelium-dependent vasodilation in the aorta and an*

Downloaded from https://academic.oup.com/cardiovascres/advance-article/doi/10.1093/cvr/cvab306/6383136 by Uniwersytet Jagiellonsky w Krakowie user on 10 November 2021

857 *increase in endothelial permeability ($p < 0.01$) (early phase of endothelial dysfunction). At the end stage*
858 *of HF, a number of RBC indices were greatly altered, including MCV ($p < 0.0001$), RDW ($p < 0.05$),*
859 *RBC shape ($p < 0.0001$), RBC deformability ($p < 0.01$), and oxidative stress (increased GSH/GSSH*
860 *ratio, $p < 0.05$) (advanced phase of erythropathy), and were associated with an advanced phase of*
861 *endothelial dysfunction, characterized not only by functionally impaired endothelium-dependent*
862 *vasodilation and increased endothelial permeability ($p < 0.05$) but also impaired NO production ($p <$*
863 *0.05), increased superoxide anion ($O_2^{\bullet -}$) ($p < 0.05$), and increased eicosanoid ($p < 0.05$) production.*
864

Downloaded from https://academic.oup.com/cardiovascres/advance-article/doi/10.1093/cvr/cvab306/6383136 by Uniwersytet Jagiellonsky w Krakowie user on 10 November 2021

Table_1

	4-m		8-m		10-m		12-m	
	FVB	**Tgαq*44**	**FVB**	**Tgαq*44**	**FVB**	**Tgαq*44**	**FVB**	**Tgαq*44**
BODY MASS [g]	24.21±1.47	25.309±1.391	27.28±2.46	28.65±2.28	29.49±2.46	30.95±3.08	29.95±2.90	26.83±2.1*
BIOCHEMICAL PARAMETERS								
TC [mmol/l]	2,680±0,271	3.019±0.366	2.41±0.29	2.84±0.66	2.97±0.28	2.6± 0.42	3.21±0.28	2.51±0.26*
HDL [mmol/l]	1.07±0.11	1.263±0.192	0.97±0.14	1.18±0.24	1.31±0.09	1.12±0.20	1.33±0.137	1.04±0.13*
LDL [mmol/l]	0.2±0.02	0.197±0.021	0.2±0.06	0.18±0.08	0.20±0.03	0.19±0.03	0.19±0.02	0.2±0.03
TG [mmol/l]	2.03±0.42	2.581±0.847	3.02±0.780	2.73±1.485	2.76±0.357	2.839±0.568	2.59±0.364	2.921±1.128
Creatinin [µmol/l]	20.16±3.93	18.471±2.766	21.31±3.76	17.62±3.65	19.2±3.63	20.69±2.31	19.23±2.95	24.97±5.49
Urea [mmol/l]	6.77±2.06	7.753±0.99	8.50±0.73	8.84±1.12	8.49±1.47	8.41±2.23	8.15±1.41	12.50±1.42**
BLOOD COUNT								
WBC [K/µl]	3.61±0.659	3.291±1.075	4.02±1.254	4.02±1.701	3.24±0.821	3.59*±0.9453	2.77±0.785	3.33±1.08
PLT [K/µl]	1209.85±102.25	1244.273±95.289	1159.08±120.86	1298.75±160.3	1050±174.018	1285.92*±212.7394	1217.17±81.13	1345.58±157.29
RBC [M/µl]	9.59±0.413	10.081±0.448	9.811±0.246	9.851±0.330	10.420±0.812	10.26±0.675	9.18±0.66	9.66±0.60
HGB [g/dl]	14.21±0.705	14.455±0.611	14.91±0.434	14.3±0.47	15.61±1.081	14.46±0.85	14.47±0.819	13.72±0.82
HCT [%]	52.284±2.388	54.2±2.603	54.133±1.444	53.1±1.82	56.882±4.177	53.93±3.55	50.65±3.61	51.47±2.97
MCHC [g/dl]	27.185±0,40	26.67±0.41	27.53±0.72	26.89±0.39*	27.42±0.41	26.59±0.23**	28.29±0.42	26.65±0.27****
NO METABOLIMS								
NO_2^- [µM]	2.09±0.46	2.03±0.51	1.21±0.52	1.20±0.18	1.48±0.39	1.16±0.42	1.03±0.37	1.04±0.49
NO_3^- [µM]	30.71±11.23	30.63±8.85	14.70±10.09	11.22±2.91	23.66± 8.14	11.90±3.72*	23.46±3.96	10.41±3.83*
HbNO [arb u]	602.85± 117.14	448.06±54.994*	335.35±135.2	230.62±103.19	461.629±135.39	362.659±123.26	505.967±189.09	226.959±79.75***

nloaded from https://academic.oup.com/cardiovascres/advance-article/doi/10.1093/cvr/cvab306/6383136 by Uniwersytet Jagiellonsky w Krakowie user on 10 November

Figure_1 Click here to access/download;Figure(s);Figure_1.tiff

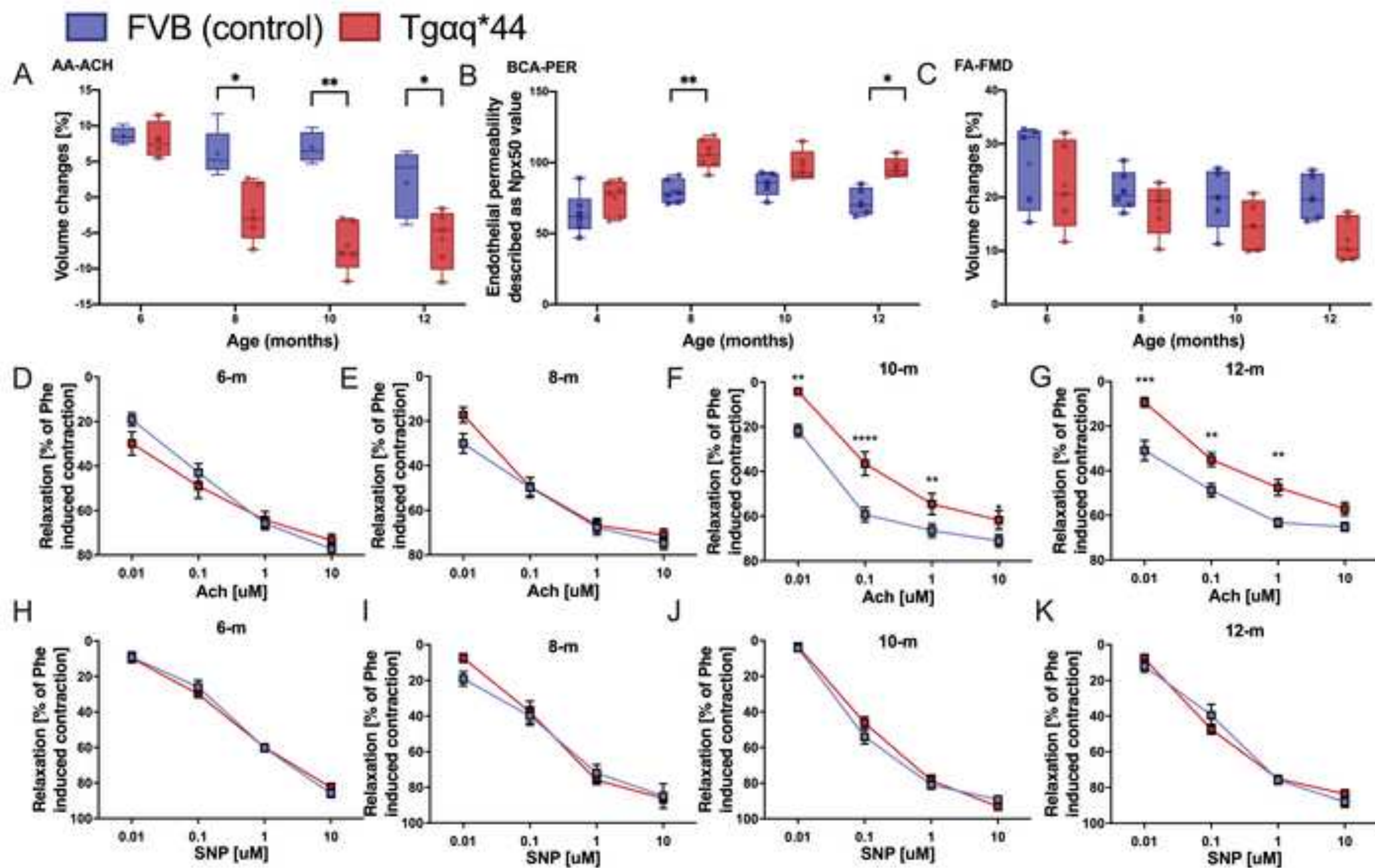

Downloaded from https://academic.oup.com/cardiovascres/advance-article/doi/10.1093/cvr/cvab306/6383136 by Uniwersytet Jagiellonsky w Krakowie user on 10 November 20

Figure_2

Click here to access/download;Figure(s);Figure_2.tiff

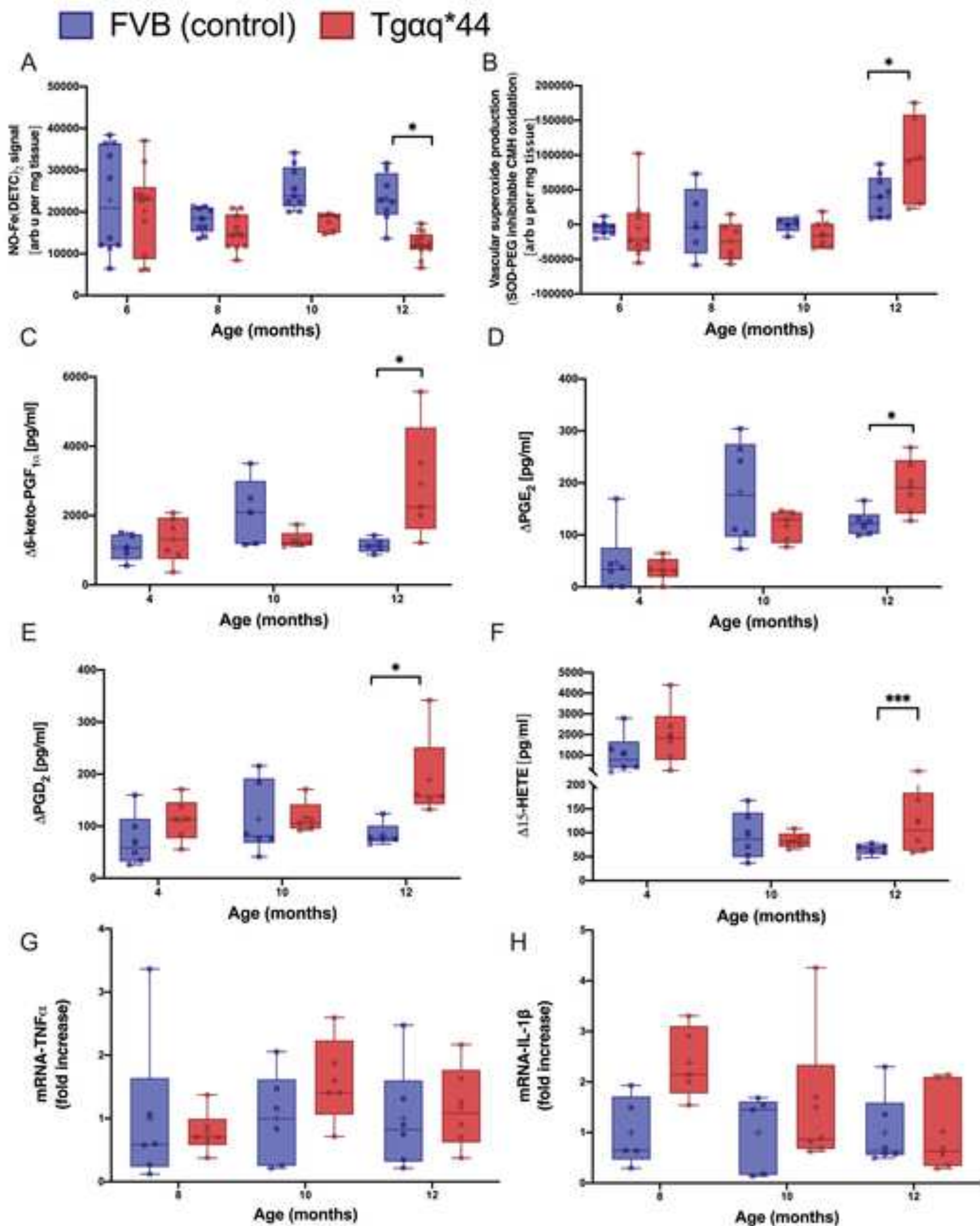

Downloaded from https://academic.oup.com/cardiovascres/advance-article/doi/10.1093/cvr/cvab306/6383136 by Uniwersytet Jagiellonsky w Krakowie user on 10 November 2021

Figure_3 Click here to access/download;Figure(s);Figure_3.tiff

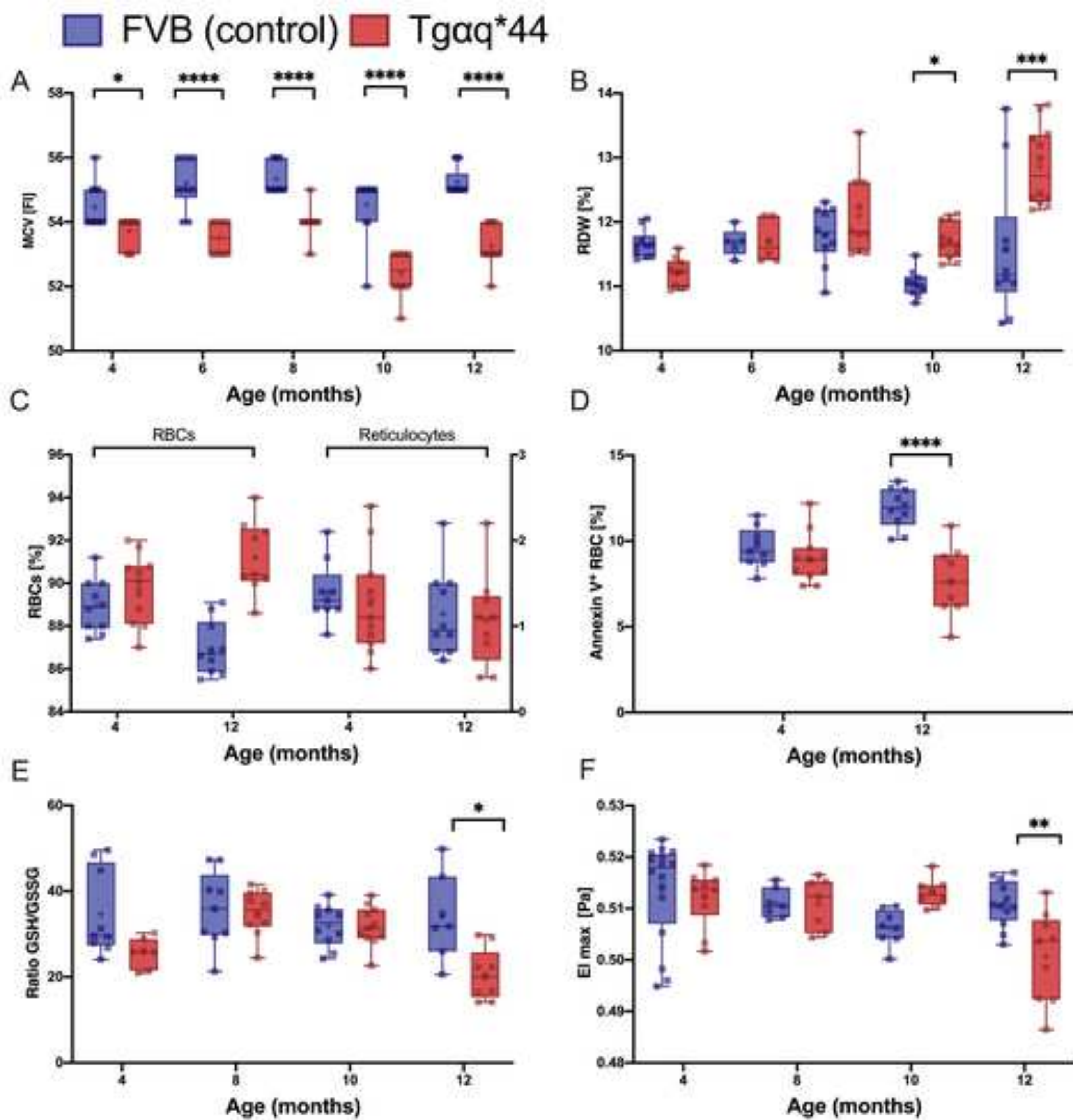

Downloaded from https://academic.oup.com/cardiovascres/advance-article/doi/10.1093/cvr/cvab306/6383136 by Uniwersytet Jagiellonsky w Krakowie user on 10 November 2021

Figure_4

Click here to access/download;Figure(s);Figure_4a.tiff

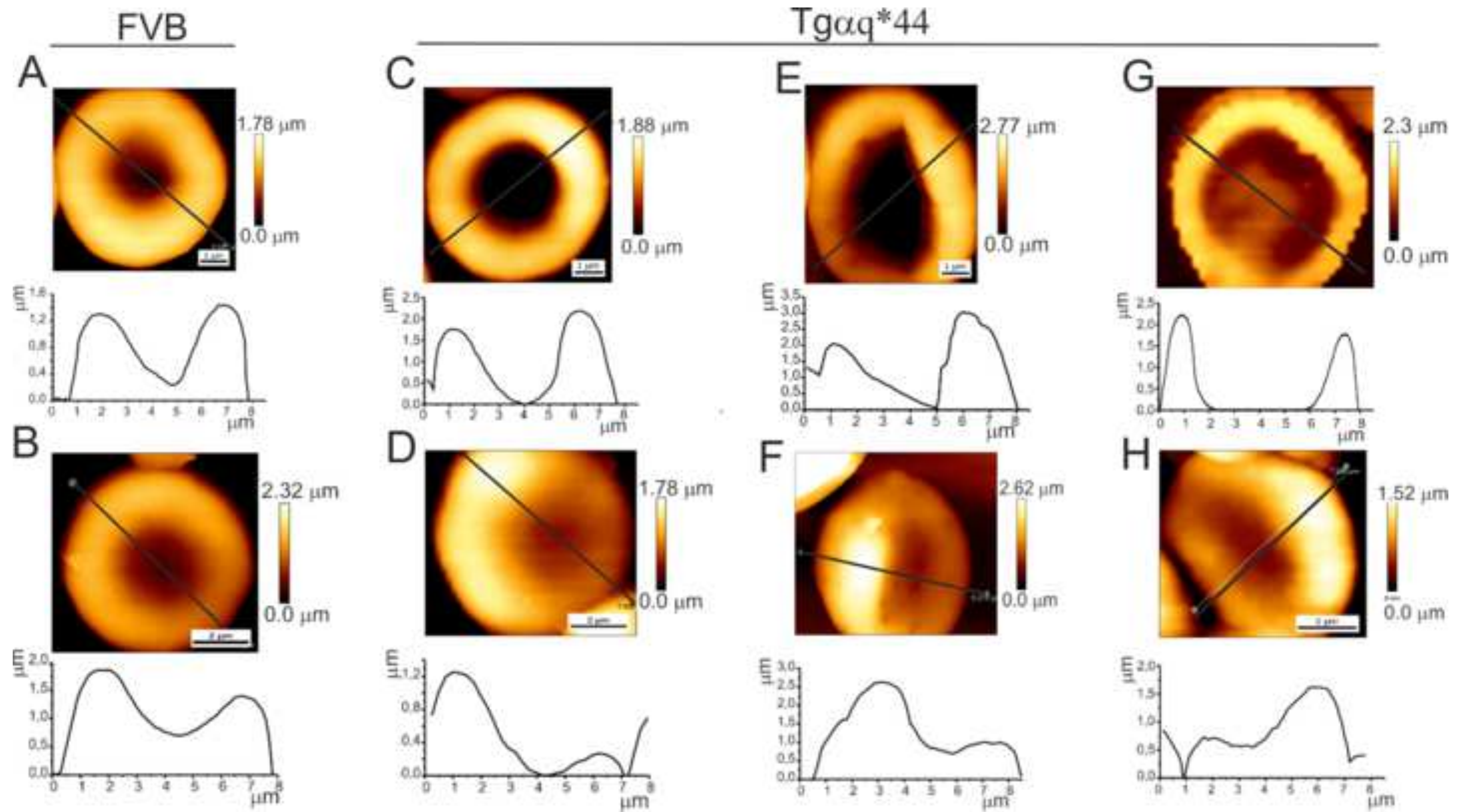

Downloaded from https://academic.oup.com/cardiovascres/advance-article/doi/10.1093/cvr/cvab306/6383136 by Uniwersytet Jagiellonsky w Krakowie user on 10 November 20

Figure_5

Click here to access/download;Figure(s);Figure_5 .tiff

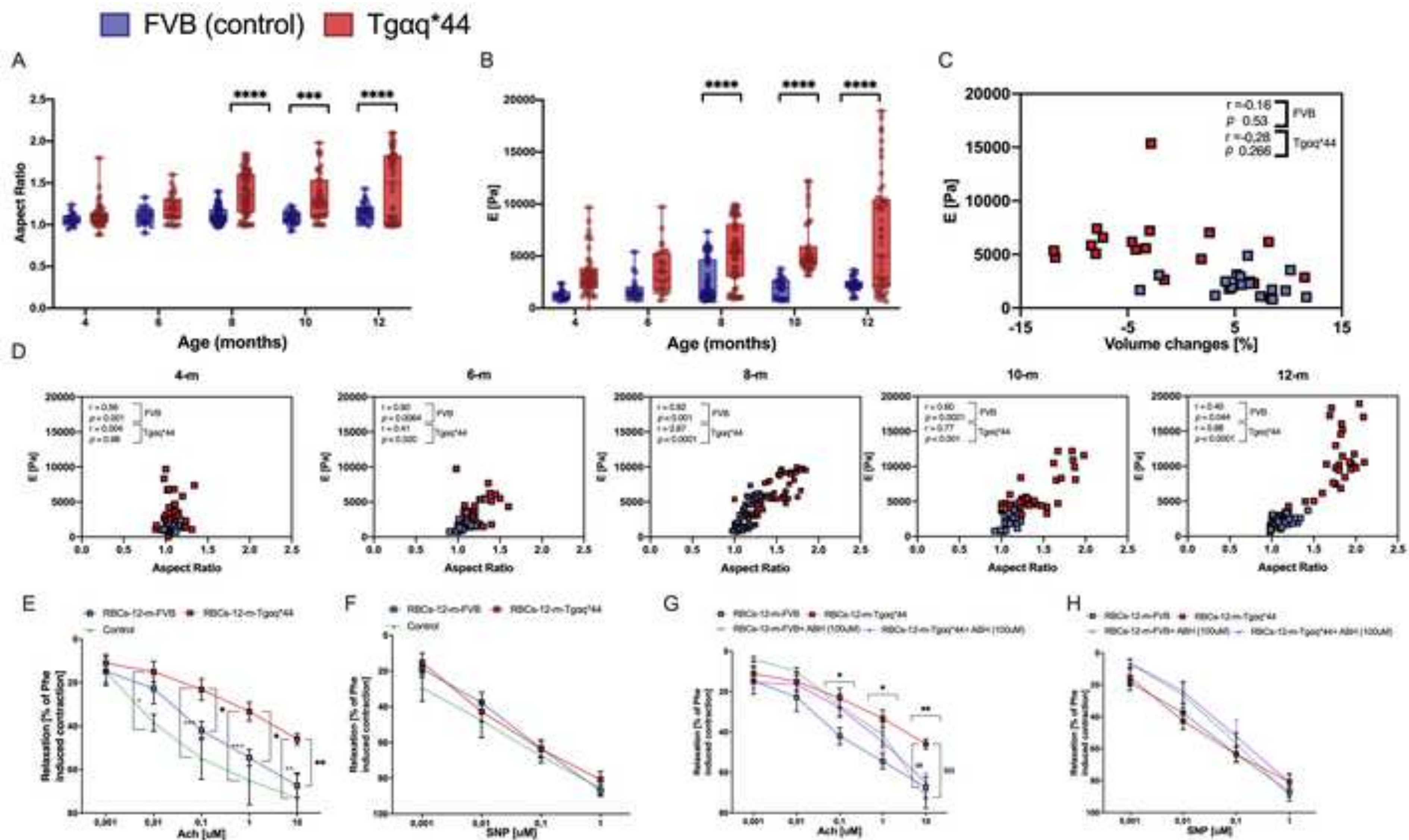

Downloaded from https://academic.oup.com/cardiovascres/advance-article/doi/10.1093/cvr/cvab306/6383136 by Uniwersytet Jagiellonsky w Krakowie user on 10 November 20

Figure_6
Click here to access/download;Figure(s);Figure_6.tiff

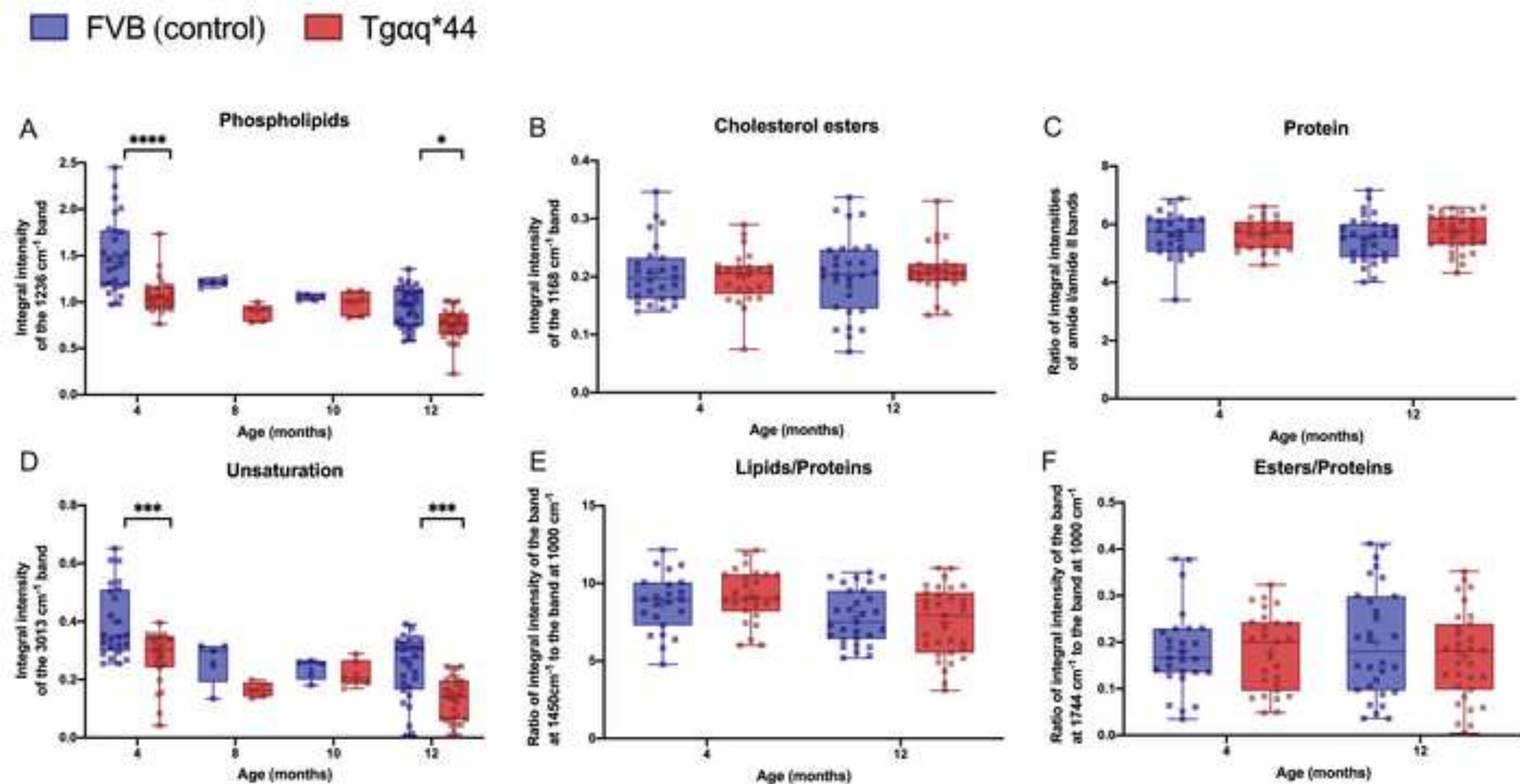

Downloaded from https://academic.oup.com/cardiovascres/advance-article/doi/10.1093/cvr/cvab306/6383136 by Uniwersytet Jagiellonsky w Krakowie user on 10 November 20

Figure_7

Click here to access/download;Figure(s);Figure 7 (Graphical Abstact) .tif

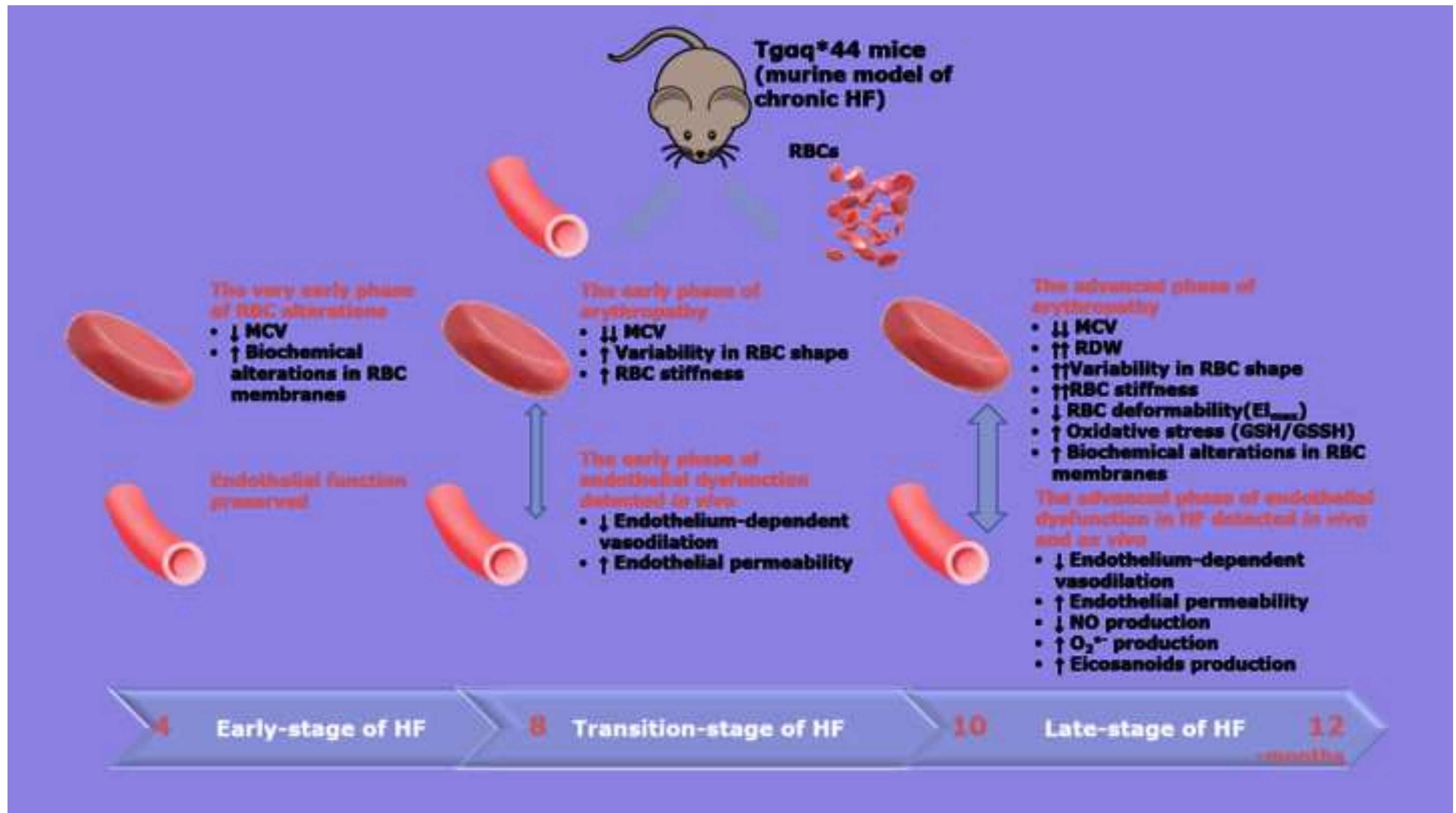

Downloaded from https://academic.oup.com/cardiovascres/advance-article/doi/10.1093/cvr/cvab306/6383136 by Uniwersytet Jagiellonsky w Krakowie user on 10 November 20

Graphical Abstract

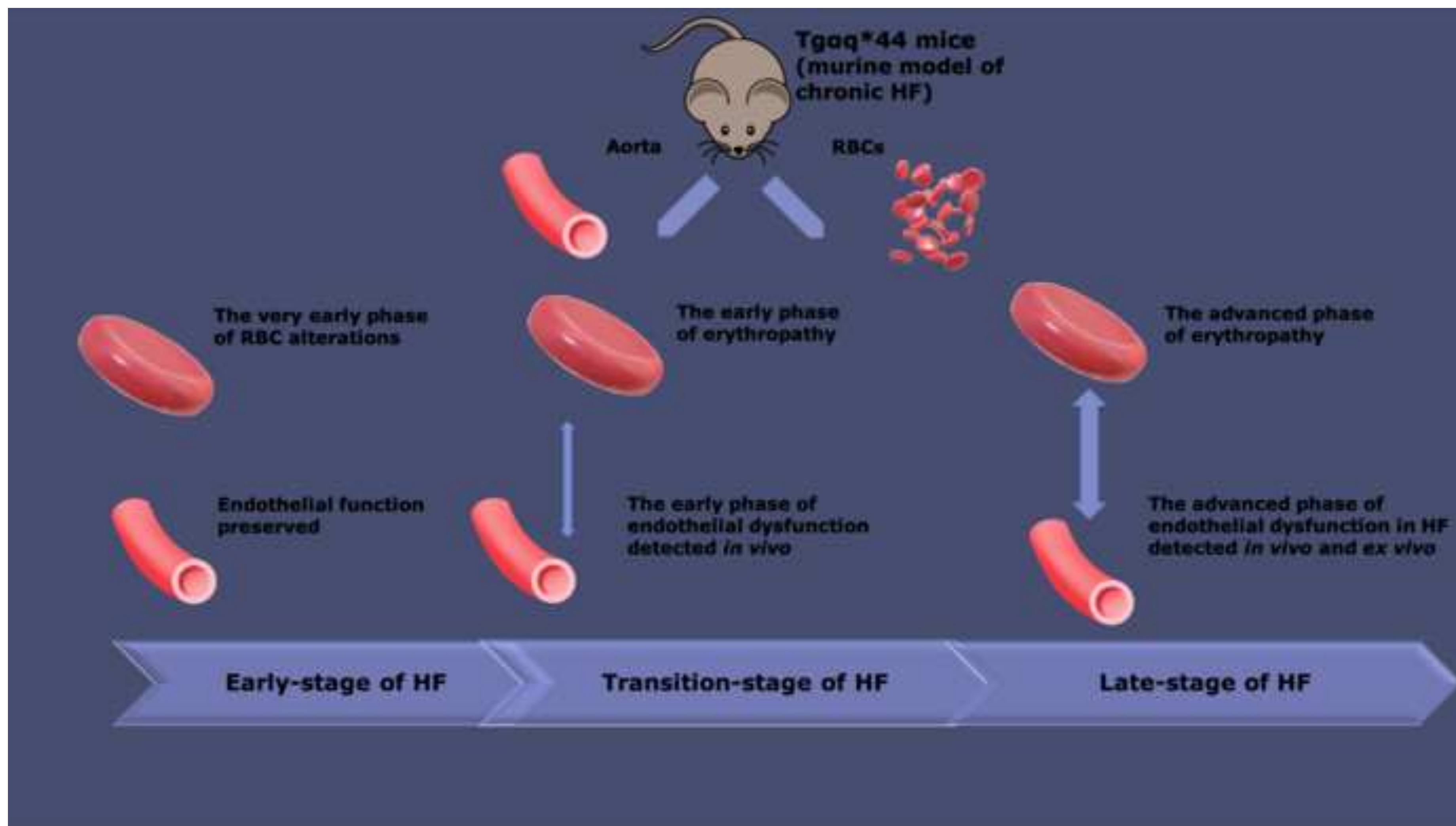

Downloaded from https://academic.oup.com/cardiovascres/advance-article/doi/10.1093/cvr/cvab306/6383136 by Uniwersytet Jagiellonsky w Krakowie user on 10 November 20